Stochastic Geometry for Mobility-Aware Performance Modeling in 6G Multi-band Wireless Networks

Md Tanvir Hossan

A thesis submitted to the
Department of Electrical Engineering and Computer Science
in conformity with the requirements for
the degree of Master of Applied Science

YORK UNIVERSITY
TORONTO, ONTARIO

April 2021

Abstract

Using tools from stochastic geometry, I develop a stochastic geometry-based tractable framework to analyze the performance of a mobile user in a two-tier wireless network operating on sub-6GHz and terahertz (THz) transmission frequencies. Specifically, using an equivalence distance approach, I characterize the overall handoff (HO) rate in terms of the horizontal and vertical HO probability. In addition, I characterize novel coverage probability expressions for THz network in the presence of molecular absorption noise and highlight its significant impact on the users' performance.

Specifically, I derive a novel closed-form expression for the Laplace Transform of the cumulative interference in the presence of molecular noise observed by a mobile user in a hybrid RF-THz network. Furthermore, I provide a novel approach to derive the conditional distance distributions of a typical user in a hybrid RF-THz network. Finally, using the overall HO rate and coverage probability expressions, the mobility-aware probability of coverage has been derived in a hybrid RF-THz network.

The mathematical results validate the correctness of the derived expressions using Monte-Carlo simulations. The results offer insights into the adverse impact of users' mobility and molecular noise in THz transmissions on the probability of coverage of mobile users. The results demonstrate that a small increase in the intensity of THz base-station (TBSs) (about 5 times) can increase the HO probability much more

compared to the case when the intensity of RF base-station (RBSs) is increased by 100 times. Furthermore, I note that high molecular absorption can be beneficial (in terms of minimizing interference) for dense deployment of TBSs and the benefits can outweigh the drawbacks of signal degradation due to molecular absorption.

Acknowledgments

Foremost, I would like to express my earnest gratefulness to my advisor Professor Hina Tabassum for the enormous support during my study and enhancing my knowledge in the field of wireless communications. Her reviews, insightful comments, encouragement, and legitimate guidelines aided me to develop the contents of my research work. Furthermore, I would like to thank my thesis board members, Professor Gene Cheung and Professor Mehdi Nourinejad, who gave their valuable feedback.

I would like to acknowledge York University along with the Department of Electrical Engineering and Computer Science for providing me a chance to study in a student friendly environment.

In addition, this is a great opportunity for me to be a graduate in Electrical Engineering and Computer Science, where I had a chance to enrich my research expertise profoundly. I also want to express my appreciation from the deep of my heart to lab members, especially Sheyda Zarandi, Sadeq Bani Mehem, and Javad Sayehvand for their unconditional support. I want to provide my acknowledgement to all of my Bangladeshi groups living in Canada, for their endless care and support during my study in Canada.

Finally, I must express my very insightful gratitude to my beloved mother, my sister and grandmother for providing me with trustworthy support and continuous

reassurance throughout my years of study and through the process of researching and writing thesis. This achievement would not have been conceivable without them.

Contents

List of Figures

Chapter 1

Introduction

1.1 6G and its Evolution:

The "G" in mobile communications denotes the "Generation" of telephone network standards and technological implementations. The evolution was started with 1G in 1979 and now we are in the era of fifth generation (5G) networks. Each cellular generation is designed to improve the reliability of wireless connections and the volume of data rates on the basis of customers' demands. With the recent release of 5G-new radio (NR) standard, early 5G deployment has already started in various countries including South Korea, Canada, and China. The deployment of 5G will take the annual GDP growth of Canada to $40B and create 250K permanent jobs by 2026. [1].

5G-NR has a multitude of advantages over the long-term evolution (LTE)/ LTE-advanced technology, i.e., higher data rates ($\sim$ 0.1 Gbps), low latency ($\sim$ 1 - 10 msec), higher mobility ($\sim$ 500 km/h), and support to 10^6 devices per sq. km. The use-cases of 5G-NR include ultra-reliable low latency communication (uRLLC), enhanced mobile broadband (eMBB), and massive machine-to-machine communication (mMTC) that

leverage on three disruptive technologies, i.e., millimeter-wave (mmWave) communication, large-scale antenna arrays (i.e., massive MIMO), and ultra-dense deployment of access points. Subsequently, a variety of exhilarating applications are emerging, such as intelligent transportation, e-health, agriculture, virtual/augmented reality (VR/AR), and rural connectivity. Despite the aforementioned advancements, the global mobile traffic volume is expected to grow from 7.462 EB/month in 2010 to 5016 EB/month in 2030 [2]. Thus, the launch of the sixth generation (6G) wireless networks are inevitable. The key performance indicators of 6G are listed as follows [3]:

- *Data rate:* The peak data rate is expected to be at least 1 Tbps which is 100 times more than 5G [2]. For specific applications, such as terahertz (THz) wireless backhaul and front-haul (x-haul), the peak data rate can reach up to 10 Tbps. A user-experienced data rate can range from 1 - 10 Gbps, which is higher than 5G.

- *Latency:* Latency will be in the order of $<$ 1ms [3] and can go up to 10 µs for the industrial IoT applications. An over-the-air (OTA) latency of 10–100 µs is targeted in 6G, as compared to the latency of 1 to 10 ms in 5G.

- Connectivity and Capacity: 6G will support 10 to 100 times connections (trillions of devices) than 5G.

- *Volumetric Spectral and Energy efficiency:* Due to integrated terrestrial-aerial network in 6G, the network spectral-energy efficiency will be defined over a specific volume in km^3. The energy efficiency in 6G is expected to improve by 10 to 100 times than 5G.

Table 1.1: The key characteristic comparison between 5G and 6G

Key Characteristic	**5G**	**6G**
Area Traffic Capacity	0.01	1 Gbps/m^2
Network Energy Efficiency		100 times than IMT-2020 (5G)
Connectivity Density (Devices/km^2)	10^6	10^7
Latency (ms)	1-10	0.01 - 0.1
Mobility (Km/h)	500	$\geq$ 1,000
User-Experienced Data Rate (Gbps)	0.1	1
Per device peak-data rate (Tb/s)	0.02	$\geq$ 1

The era of 6G will connect each and every device and the term "internet-of-everything" will become popular over "internet-of-thing" [3]. To deal with high data rate in evolving wireless applications, THz frequencies (up to 3THz) would be a potential candidate for 6G networks. International Telecommunication Union formed a group named "Network 2030" to search new technologies for 6G. In table 1.1, a comparison of the key characteristics of 5G and 6G networks is presented.

Furthermore, 6G networks will accommodate different communications modes from satellite-ground to underground. Therefore, modeling the mobility of users and base stations would be crucial. Note that the satellites, unmanned-aerial-vehicles, and ground users will have mobility. On top of it, the use of high frequencies exacerbates the hand-off and mobility related issues as the coverage areas shrink. In Fig. 1.1, the vision of 6G in coexisting radio frequency (RF), mmWave, THz, and optical wireless communication networks has been illustrated.

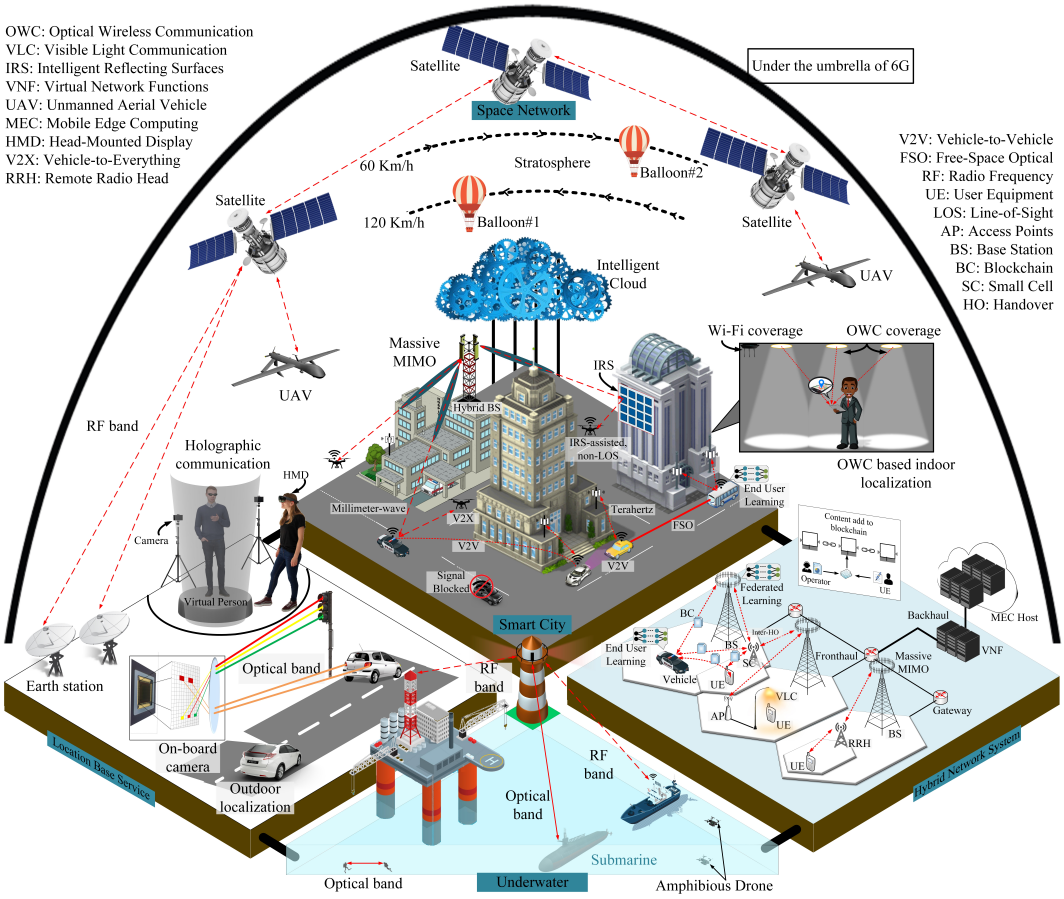

Figure 1.1: Vision of 6G in Multi-band Networks.

1.2 Terahertz Communication in 6G

While the sub-6GHz frequency bands offer wider coverage area, its low transmission rate is a challenge in the era of high speed communication. In addition, accumulation of the mmWave band in 5G is still lagging behind in coping up with the bandwidth requirements. In order to resolve this issue, another band of frequency has to be searched from the electromagnetic spectrum for communication purposes [4]. To date, the THz spectrum which lies in between the mmWave and the optical spectrum

has been investigated rarely. However, with the recent innovations in THz signal generation, radiation, and modulation methods, the so-called THz gap is closing. THz spectrum can support massive data rates in the order of hundreds of Gigabits-per-second (Gbps), massive connectivity, and extremely secure transmissions. The narrow directed THz transmission makes it ideal for point-to-point communications, which is important to convey the information securely. Also, when the dense deployment of sub-6GHz spectrum will cause unnecessary interference, THz access points may clear the difficulties. In addition, THz frequency band could be used where the scope of wired network is very limited and costly [4]. In this context, multiple leading 6G initiatives probe THz communications, including the "6Genesis Flagship Program", the European Commission's H2020 ICT-09 THz Project Cluster, and the "Broadband Communications and New Networks".

Nevertheless, channel propagation at THz frequency is susceptible to molecular absorption due to oxygen molecules and water vapor absorption. Specifically, a part of electromagnetic energy gets transformed into the internal energy of molecules, referred to as molecular absorption noise which is a function of frequency [5]. To determine the amount of THz radiations that are capable of penetrating through the absorbing medium, the transmittance from the Beer–Lambert's law is typically applied. There are two major challenges that THz based wireless communication faces, i.e., molecular absorption loss and spreading loss [4]. A fraction of THz signal energy is typically transformed into the kinetic energy of the air molecule known as *molecular absorption loss* of THz signal. On the other hand, spreading loss of THz signal is caused by the expansion of the electromagnetic wave in the space. This loss increases significantly with the operating frequency and distance between two nodes.

1.3 Multi-band Networks in 6G

Conventional RF spectrum is characterized with strong transmission powers and wider coverage; however, the spectrum is limited and extremely congested. Evidently, THz networks have reduced coverage, but plenty of spectrum, so a trade-off in users' channel quality and available spectrum exists. As such, analyzing the performance of *multi-band* networks, e.g., coexisting RF and mmWave deployments [6], coexisting RF and visible light communication (VLC) [7,8] deployments, and coexisting RF and dense THz network [9] is crucial for 6G networks. Furthermore, due to unique channel propagation and molecular absorption losses, the THz transmissions are susceptible to smaller coverage zones; thereby resulting in frequent handoffs (HOs) even for users with low mobility. Subsequently, it is imperative to analyze the performance of *multi-band wireless networks* in the presence of *users' mobility*.

1.4 Vehicular Communication in 6G

Connected and autonomous vehicles (CAVs) are becoming crucial nowadays to improve the driving safety, ameliorate travel efficiency through efficient parking and routing, and minimize traffic congestion. Connected vehicles refer to the wireless connectivity-enabled vehicles that can communicate with their internal and external environments, i.e., supporting the interactions of vehicle-to-sensor on-board (V2S), vehicle-to-vehicle (V2V), vehicle-to-road infrastructure (V2R), and vehicle-to-Internet (V2I) [10]. The market value of autonomous transportation systems is around 7 trillion USD, which will be accommodated by next generation wireless communications technology. Technologies within 6G allow the autonomous vehicles to connect with other autonomous vehicles and ensure road safety (e.g., collision detection, lane

change warning, and cooperative merging), smart and green transportation (e.g., traffic signal control, intelligent traffic scheduling, and fleet management), and location-dependent services (e.g., route optimization).

In this context, URLLC is necessary to enable the exchange of real-time information between vehicles, and vehicle to infrastructure; thereby enabling vehicles (or drivers) to make informed decisions. However, unfortunately, while the conventional sub-6GHz network benefits from strong transmission powers and wider coverage zones, it may not guarantee URLLC due to extremely limited and congested spectrum. In the sequel, transmissions at mmWave ($\sim$ 30 - 100GHz) and THz ($\sim$ 0.1 - 10 THz) frequencies will complement traditional wireless transmissions at RF in 6G to support ubiquitous vehicular communications.

1.5 Challenges: THz-enabled Vehicle Communication

Some of the primary challenges of high frequency vehicular communication are listed as follows:

- **Network Deployment:** In vehicular communications, it is required to have high reliability and low latency. However, a high frequency band like THz in 6G has a sensitivity to blockages and high absorption losses; therefore dense THz deployments will be necessary [3]. Nevertheless, dense deployments may cause interference; therefore, it is crucial to model the interference in the presence of molecular noise and analyze its impact on the key performance metrics such as coverage probability. Also, a comprehensive analysis is required to understand the network parameters and conditions under which the THz network can become interference limited. Furthermore, although the frequent deployment of

high frequency BSs may not yield high interference, it can result in significant deployment and operational expenditures. This issue can be resolved by having selected deployment of BSs with hybrid frequencies.

- **Handoff and Mobility Management:** In 6G, BSs will have varying transmission frequencies, coverage zones, LOS connectivity, and transmission powers. Frequent installation of the BSs will cause unnecessary HOs thereby reducing the achievable throughput for vehicular communications. It is crucial to have new mobility related performance metrics that can precisely calculate the impact of HO delays and HO cost on the overall network throughput. A possible solution to cope up with the unnecessary HOs is to enable the devices' operation for multi-band connectivity, devise efficient HO skipping mechanisms, and have BSs with hybrid transmission frequencies. In high mobility scenarios, there shall be quite frequent HOs, thus new HO algorithms are needed to manage mobility properly, especially for the recent development of hybrid/co-existing networks. Proper mobility management allows to reduce the number of HO, HO latency, and the HO failure probability [11].

- **Advanced Signal Processing:** Sophisticated signal processing algorithms will be required to minimize multi-user interference and inter-carrier interference in vehicular networks. While in 6G, the number of mobile users will be more than ever. In vehicular networks, vehicles will not only connect with road side units or cloud, but also its neighbouring vehicles. Therefore, enormous data will be accessed by different mobile users, which definitely requires advanced signal processing techniques.

- **Fading Channel:** The large Doppler spread will cause fast time-variation of the fading channel for highly mobile communications [11]. The highly mobile user causes an impact on time-varying Doppler spreads and non-stationary fading coefficients. The non-stationary properties of the fading channel, along with the fast changing scattering environment, make it a challenging task to predict, estimate and track the fast time-varying fading coefficients perfectly [12].

- **Accurate Channel Estimation:** Channel estimation is a non-trivial task in high mobility systems, and the estimation performance might have significant impacts on the overall system performance. In many high mobility systems, channel estimation errors are inevitable and they will seriously degrade system performance. The common assumption of perfect CSI adopted for the design of low mobility systems is no longer valid for high mobility systems. Thus the designs of high mobility transceivers need to take into considerations of the properties of channel estimation errors. Alternatively, non-coherent systems that do not require the knowledge of CSI can be developed for high mobility systems [12].

- **Doppler Diversity:** Even though fast time-varying fading will degrade system performance, the short coherence time and fast variation of the fading channel also provide Doppler diversity, which can be exploited to improve system performance. Doppler diversity has been studied extensively for systems with perfect CSI. However, considering imperfect CSI is crucial in high mobility systems and therefore statistical modeling is crucial [12].

- **Carrier Frequency Offset:** The Doppler shift at the received signal can cause

a mismatch between the frequencies of the oscillators at the transmitter and receiver, and this is called the carrier frequency offset (CFO). In multi-carrier systems, CFO destroys the orthogonality among the sub-carriers, and introduces inter-carrier interference [12].

1.6 Thesis Contribution

In this thesis, I investigated the problem of HO rate modeling and coverage analysis for two-tier hybrid RF-THz network. My contributions can be listed as follows:

- I characterize the overall HO rate (which is based on the vertical and horizontal HO rate) of a mobile user in the downlink of a hybrid RF-THz network, considering the maximum received signal power association criterion. In this context, an *equivalence distance approach* is applied by introducing a virtual tier with the serving tier of a mobile user in order to facilitate the analysis of vertical HO. In addition, I pointed out that a correction factor is missing in the HO probability expressions of all aforementioned research works (whether single-tier or multi-tier) related to mobility [13–15].

- I analyze the exact coverage probability of a typical user in the THz networks considering the impact of molecular noise absorption and highlight the devastating impact of ignoring the molecular absorption noise on the coverage probability. Specifically, I derive a new closed-form expression for the Laplace Transform of the cumulative molecular noise and interference observed by a typical user in a stand-alone THz or a hybrid RF-THz network.

- I provide a novel approximation to derive the conditional distance distribution

of a typical user in a hybrid network. Note that the mathematical model of a THz channel is mathematically challenging due to Beer's Lambert transmission model. Therefore, compared to [9], I propose a novel and efficient approximation to make the framework tractable.

- Using the overall HO rate and coverage probability expressions, I derive the *mobility-aware probability of coverage* of a mobile user in a hybrid RF-THz network.

- Numerical results validate the accuracy of my derived expressions. The results offer insights into the impact of mobility and molecular noise on the probability of coverage of mobile users in a stand-alone THz and hybrid network. Also, the results signifies the impact of molecular absorption and intensity of BSs on the HO rate and the mobility-aware coverage probability.

Remark: The proposed theoretic framework does not require instantaneous CSI as it applies the mathematical channel models that are realistic and well-recognized in terms of modeling the BS locations, channel fading, etc. These statistical models are then used to derive the mobility-aware performance metrics.

1.7 Research Outcomes

The outcome of this thesis is submitted to "IEEE Transactions on Communications", which is under review. In addition, I have another publication in a conference, which is my initial work on hybrid RF-THz network [16].

Chapter 2

Background and Literature Review

In this chapter, I will cover the review of the relevant research works and classified them in the categories such as performance of THz networks without mobility and with mobility. Then, I reviewed the research works related to the performance of multi-band networks with and without mobility.

2.1 Performance of THz Networks without Mobility

The existing research works considered analyzing the performance of a given THz transmission link [17] or THz-only network [18, 19]. For instance, the authors in [17] derived a closed-form expression of the outage probability and ergodic capacity considering a THz wireless fiber extender system (i.e., a single transmission link) with ideal and non-ideal RF front-end. In [18], the authors characterized the average interference in a stand-alone THz network by applying the methods from the stochastic geometry assuming an interference-limited regime. However, the closed-form expression of the average interference was not applied to the coverage or outage analysis of a typical user. Instead, the interference distribution was approximated with a log-logistic distribution to compute the coverage probability. The authors highlighted

that the application of the log-logistic approximation may not always be precise.

In [19], the authors analyzed the reliability and end-to-end latency considering a THz-only network with a finite number of BSs. The interference distribution was approximated with a normal distribution. Likewise, in [20], the the interference was approximated with the average interference. In [21], the authors derived connection probability and the ergodic capacity of a user for two multi-connectivity strategies in a stand-alone THz network. However, the impact of interference on the coverage probability was not considered.

In [22], the interference and outage probability in a THz-only network was investigated. The interference was approximated with mean interference. The authors in [23] derived the approximate coverage expressions for a single-tier network, where RBS or TBS can be used in an opportunistic manner. However, given the small coverage of THz transmissions, it is practical to consider a two-tier network with a separate denser deployment of TBSs than the deployment of RBSs.

Research Gap: The aforementioned research works considered standalone THz networks and ignore the impact of mobility on the performance metrics such as coverage probability and data rate.

2.2 Performance of Wireless Networks with Mobility

To date, several research works have considered the impact of mobility in wireless networks. However, there are a handful of research works that considered mobility-aware performance characterization of large-scale wireless networks using stochastic geometry. There are two streams of research works with different definitions of HO event. The first stream is referred to as *trajectory-based HO* where the HO occurs

when the moving user travels across cell boundaries of different BSs along its trajectory. The HO probability is based on evaluating the number of intersections on the user's trajectory and the set of cell boundaries. The second stream is referred to as *association-based HO* where the HO occurs when a user finds a better BS in terms of signal quality (compared to its serving BS).

Regarding the first stream, the authors in [24] applied a modified random way point (RWP) mobility model in a Poisson point process (PPP) network and derived an analytical expression for the HO rate and sojourn time. The authors considered a single-tier network with BSs modeled by a PPP and demonstrated that the HO rate is proportional to the square root of the BS density. This work defines the *HO rate as the ratio of the average number of cells a mobile user traverses to the average transit time (including the pause time).* In [25], the authors use stochastic geometry to develop a tractable mobility-aware model for a two-tier downlink cellular network with ultra-dense small cells and separated control plane-user plane split network architecture. The macro cells in their proposed architecture act as HO anchors and only inter-macro HOs are reported to the core network. As a result, both control overheads and HO delays are significantly reduced. The overall throughput gains of HO skipping were observed due to HO delay reduction. The authors assumed every time a mobile user crosses a cell boundary that a HO is always completed, however, they do not compare quantitatively how much signalling load is generated in case of HO success or HO failure. The assumption that path loss exponents in different tiers are the same is not practical when quantifying the effect of mobility.

To date, several research works have considered the impact of mobility in wireless

networks using RF spectrum. However, there are handful of research works that considered mobility-aware performance characterization of large-scale wireless networks using stochastic geometry. Regarding the second stream, in [13], the HO probability analysis was conducted in a multi-tier cellular network. The authors showed that there is an impact of users' mobility on tier association and coverage probability. Nevertheless, the framework in [13] only deals with the horizontal HO (i.e., the HO between the BSs in the same tier). This shortcoming arises because the closest BS to the user after HO is always considered as the new serving BS, which is not true in multi-tier networks with BSs having distinct powers, coverage zones, and operating frequencies. To overcome this shortcoming, in [14,15], the authors showed an equivalence analysis to analyze both the vertical and horizontal HO probabilities considering a two-tier RF networks. It is noteworthy that there is a correction factor that needs to be included in the HO probability expressions of all of the aforementioned research work related to mobility as is shown in [26].

Research Gap: None of the aforementioned research works analyzed the impact of mobility in high frequency networks.

Recently, There are other research works find, where different forms of a PPP is describing the mobility or mobility management especially in a vehicular environment. A Poisson line process (PLP) is used to model the road network and, conditionally on the lines, linear Poisson point processes are used to model the vehicles on the roads. A line process is simply a random collection of lines in a two-dimensional (2D) plane. Conventional planar base stations and users are modeled by the independent planar Poisson point processes. Cox process or doubly stochastic Poisson point process, where the roads in a network are modeled by a PLP and the location of nodes on the

Table 2.1: Similar Literature Review of Wireless Networks with Mobility

Ref.	**Contribution**	**Technique**
[27]	Analyzes cellular architecture considering two types of BSs, i.e., planar BSs (uniformly distributed in Euclidean plane), and base stations located on roads.	PLP
[28]	The roadways model are predominantly straight and randomly oriented and the locations of nodes on each road as a one-dimensional (1D) PPP	PLP, 1D PPP
[29]	Characterizes the success probability of a typical link and spectral efficiency of a vehicular ad hoc network modeled as a Cox process	Cox Process
[30]	Derive a new framework to analyze the worst-case impact of correlated blocking on the blind-spot probability of a typical target	PLP, PPP
[31]	Derive quadratic position of the points, the nearest distance distribution, the Laplace functional, the densities of facets of the Cox-Voronoi tessellation, and the asymptotic behavior of the typical Voronoi cell under vehicular densification	Cox Process
[32]	Present the downlink coverage and rate analysis of a cellular vehicle-to-everything communication network where the locations of vehicular nodes and road side units	PLP, 2D PPP
[33]	Derive a framework to analyze a wireless architecture where vehicles collect data from devices	PLP, Cox Point Process
[34]	Develop a framework to study multi-hop relaying in a vehicular network consisting of vehicles and Road Side Units (RSUs), and the effect of this relaying on the network coverage and the communication delay	PLP, 1D PPP
[35]	A stochastic geometry approach is applied to model the considered Network-NOMA scenario as a Poisson cluster process, based on which closed-form analytical expressions for outage probabilities and ergodic rates	PLP, Cox Point Process

roads are modeled by a 1D PPP. For BSs, superposition of cox process on Poisson line and planar PPP on Euclidean plane. For users, Superposition of stationary cox

process on Poisson line (i.e., for vehicle users) and stationary planar PPP on Euclidean plane (i.e., for planar user). Using Palm calculus to investigate the statistical properties of a typical user in such a network. More relevant research can be found in Table 2.1.

2.3 Performance of Multi-band Networks

Different from the existing research, very recently, [9] characterized the exact coverage probability and interference statistics of users in a stand-alone THz network and a hybrid two-tier RF-THz network with the help of stochastic geometry. Specifically, all aforementioned research works ignored the impact of mobility on the performance of THz networks as well as multi-band networks. Also, the impact of molecular absorption noise along with the cumulative interference was not considered.

Recently, a wireless system architecture with hybrid THz and RF decode-and-forward relaying system for both backhaul and fronthaul applications as studied in [36]. The authors derived the cumulative density function (CDF) of the end-to-end (E2E) signal-to-noise ratio (SNR), the outage probability, and symbol error rate (SER). However, none of the aforementioned research works quantified the impact of molecular noise and users' mobility on the coverage probability of a mobile user who is moving with a predefined velocity in a large-scale RF and THz network.

Software-defined network (SDN) may be integrated with vehicle-to-vehicle networks for supporting flexible THz protocol switching, which is shown in [37]. The authors proposed a controlled switching between mmWave and THz bands in a small cell network and provide an admission policy for dynamic switching in the small vehicular network. The SDN controller provide admission control for the adaptive

switching in the vehicles equipped with THz and mmWave devices and provides Spectrum Switching, vehicle scheduling and capacity modeling as controller components to accommodate asymmetric uplink/downlink communication. Comparing with the channel model over the regular bands where each link is in either a line-of-sight (LoS) or non-line-of-sight (NLoS) state, the adopted three-state model incorporates an additional outage state which can describe the channel blockage effect over the mmWave and THz bands. The effective capacity is measured through mathematical modeling of the available capacity in the network. The outage probability and power consumption at the transmitter are key parameters for evaluation.

Based on the stochastic geometry theory, the LoS and NLoS interference caused by vehicles on the side lanes were evaluated for mmWave and low THz bands (i.e., 79 GHz) V2V communications in three-lane highways and urban road environments in [38]. The authors showed that the interference power strongly depends on the directivity of mmWave and low THz bands antennas and interference from the adjacent lanes significantly degrade overall performance. Moreover, mmWave signals can be easily blocked by common obstacles such as, for example, vehicles, road signs, pedestrians. Additionally, the metal of the vehicle bodies acts as a strong reflector for mmWave and low THz bands, creating strong and bursty interference. The authors observed that the antenna beam widths less than 20 degrees captured minimal interference from the side-lanes such that interference management schemes were not required. However, the larger angular coverage achieved by beam widths greater than 40 degrees also captured significant interference from the side-lanes, which necessitated the use of interference mitigation schemes for reliable communications.

2.4 Summary

In this chapter, I presented a survey of scholarly sources on different wireless networks, including stand-alone RF/THz networks and/or hybrid RF-THz network. I explained about different approaches from different research articles along with the tools and the techniques in brief.

None of the aforementioned studies analyzed the performance of a mobile users in a *large-scale THz network* in the presence of *mobility* of users and *cumulative interference and molecular absorption noise*. Furthermore, there are no investigations related to the mobility-aware performance of users in a *two-tier* hybrid RF-THz network.

Chapter 3

Mobility-Aware Performance Characterization

This chapter provides a comprehensive tractable stochastic geometry framework to calculate the HO rate and its impact on the probability of coverage of a mobile user in a hybrid RF-THz network. The proposed framework is applicable not only for (i) stand-alone RF or THz system, but also (ii) hybrid RF-THz network.

Section 3.1 presents the system model, assumptions, and the methodology of analysis. The horizontal and vertical HO probability analysis is presented in Section 3.2. Section 3.3 characterizes the coverage probability of a user in the presence of molecular absorption noise and incorporates the impact of horizontal and vertical HO probability in the calculation of the mobility-aware coverage probability. Finally, selected numerical and simulation results are presented in Section 3.4 before conclusions in Section 3.5.

3.1 System Model and Assumptions

In this section, I present the spatial network deployment model, channel propagation models, and mobility/HO model of a typical mobile user in a multi-band network.

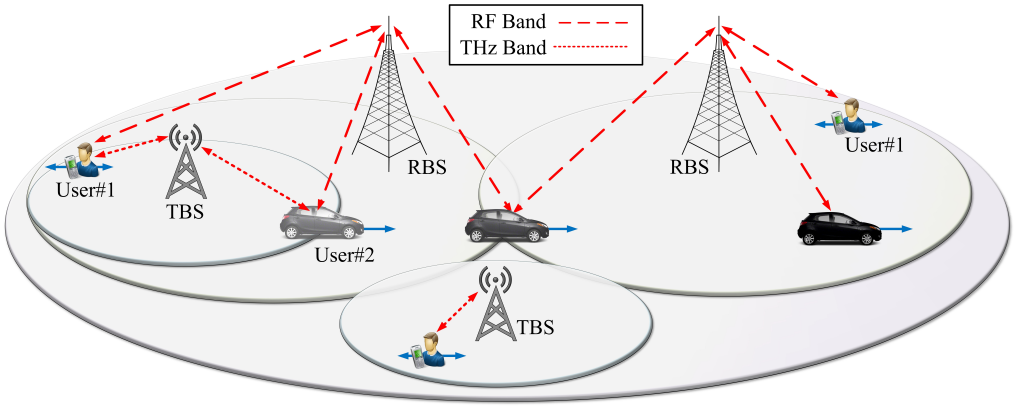

Figure 3.1: Graphical illustration of a two-tier hybrid RF-THz network with low- and high-velocity users.

Finally, I present the step-by-step methodology of analyzing the mobility-aware coverage probability.

3.1.1 Spatial Network Deployment

The RF BSs and THz BSs are comprised in a two-tier downlink network. The spatial deployment of the RBSs and TBSs is taken as a 2D homogeneous PPP $\mathbf{\Phi}_R$ and $\mathbf{\Phi}_T$ with intensities λ_R and λ_T, respectively. The users are distributed in the circular region following independent homogeneous PPP $\mathbf{\Phi}_u$ with intensity λ_u. I evaluate the performance of a mobile user who is originally found at the origin and measures the channel quality from each BS. The mobile user associates to a given BS according to maximum received signal power from that BS. An illustration of the considered network is shown in Fig. 1 where the typical mobile user can be classified according to its velocity, e.g., pedestrians with low velocity and vehicles with moderate to high velocity.

3.1.2 Mobility Model and Handoff Criterion

The typical mobile user moves with a velocity v from the origin in an arbitrary direction, thereby HO may occur depending on the maximum received signal power criterion. HOs (or association of users) can be performed based on both the instantaneous received power [39, 40] and maximum long-term averaged received power [41–45]. However, the HO based on instantaneous channel gain may yield "ping-pong effect" due to short-term instantaneous fading. To overcome this undesired phenomenon, the received signal power is averaged over the measurement period in LTE. This assumption, also has been considered in other research works [42–45] and is considered as more realistic compared to instantaneous received power based user association [45, page1]. The HOs in the same tier (e.g., RBS-RBS or TBS-TBS) are referred to as *horizontal HO*. Alternatively, when the type of user switches its BSs in two different tiers (e.g., RBS-TBS or TBS-RBS), then this HO is defined as *vertical HO*.

3.1.3 Communication Model - RF

The signal transmitted from RBS incurs path-loss and short-term channel fading which is Rayleigh distributed. At the typical mobile user, the received signal power can be defined as given below:

$$P_R^{\mathrm{rx}} = G_R^{\mathrm{tx}}\, G_R^{\mathrm{rx}} \left(\frac{c}{4\pi f_R}\right)^2 \frac{P_R^{\mathrm{tx}}}{r_0^{\alpha}}, \tag{3.1}$$

where $P_R^{\mathrm{tx}}, G_R^{\mathrm{tx}}, G_R^{\mathrm{rx}}, c, f_R, r_0$, and α denote the transmit power from the RBSs, transmitting antenna gain, receiving antenna gain, speed of the electromagnetic wave, RF carrier frequency (in GHz), initial unconditional distance between the mobile user

to the serving RBS, and path-loss exponent of the signal, respectively. The signal-to-interference-plus-noise ratio (SINR) of a typical mobile user on RF transmission channel is thus modeled as:

$$\mathrm{SINR_R} = \frac{P_R^{\mathrm{tx}}\, G_R^{\mathrm{tx}}\, G_R^{\mathrm{rx}} \left(\frac{c}{4\pi f_R}\right)^2 H}{r_0^{\alpha}\,(N_R + I_R)} = \frac{P_R^{\mathrm{tx}} \gamma_R H}{r_0^{\alpha}\,(N_R + I_R)}, \tag{3.2}$$

where H is the exponentially distributed channel fading power of the mobile user from the targeted RBS, N_R is the power of thermal noise at the receiver, $I_R = \sum_{i \in \Phi_R \setminus 0} P_R^{\mathrm{tx}} \gamma_R r_i^{-\alpha} H_i$ is the cumulative interference at the mobile user from the interfering RBSs. From the cumulative interference, r_i is the distance between the i-th interfering RBS and the typical mobile user, H_i is the power of fading from the i-th interfering RBS to the typical mobile user, and $\gamma_R = G_R^{\mathrm{tx}}\, G_R^{\mathrm{rx}}\, (c/4\pi f_R)^2$.

3.1.4 Communication Model - THz

In THz network, the LOS transmissions are much more significant than the NLOS transmissions due to the presence of molecular absorption. Subsequently, in this work, following [18, 46–48], I calculate the received power taking into account the LOS transmission property from [49], [9] as follows:

$$P_T^{\mathrm{rx}} = G_T^{\mathrm{tx}}\, G_T^{\mathrm{rx}} \left(\frac{c}{4\pi f_T}\right)^2 \frac{P_T^{\mathrm{tx}} \exp(-K_a(f_T)\, d_0)}{d_0^2}, \tag{3.3}$$

where $P_T^{\mathrm{tx}}, G_T^{\mathrm{tx}}, G_T^{\mathrm{rx}}, f_T, d_0$, and $K_a(f_T)$ denote the transmit power of the TBSs, transmitting antenna gain of the TBS, receiving antenna gain of the TBS, THz carrier frequency, initial unconditional distance between the mobile user to the serving TBS, and the molecular absorption coefficient depends on the composition of the medium

and also on the frequency (i.e., f_T) of the signal, respectively[1]. Note that $G_T^{\text{tx}}(\theta)$ as well as $G_T^{\text{rx}}(\theta)$ are directional transmitter and receiver antenna gains, respectively. The beamforming gains from the main lobe and side lobes of the TBS transmitting antenna can be generalized as follows [50]:

$$G_T^{\text{q}}(\theta) = \begin{cases} G_{\max}^q & \mid \theta \mid \leq w_q \\ G_{\min}^q & \mid \theta \mid > w_q \end{cases}, \tag{3.4}$$

where $q \in \{\text{tx}, \text{rx}\}$, $\theta \in [-\pi, \pi)$ is the the boresight direction angle, w_q is the beamwidth of the main lobe, $G_{\max}^q$ and $G_{\min}^q$ are the beamforming gains of the main and side lobes, respectively. I assume that the typical mobile user's receiving beam aligns with the transmitting beam of the associated TBS through beam alignment techniques. However, the alignment between the user and interfering TBSs is a random variable and depends on the predefined values of transmitter and receiver antenna gains. The alignment variable D can take values as:

$$D \in \{G_{\max}^{\text{tx}} G_{\max}^{\text{rx}}, G_{\max}^{\text{tx}} G_{\min}^{\text{rx}}, G_{\min}^{\text{tx}} G_{\max}^{\text{rx}}, G_{\min}^{\text{tx}} G_{\min}^{\text{rx}}\},$$

and the respective probability for each case is $F_{\text{tx}} F_{\text{rx}}$, $F_{\text{tx}}(1 - F_{\text{rx}})$, $(1 - F_{\text{tx}}) F_{\text{rx}}$, and $(1 - F_{\text{tx}})(1 - F_{\text{rx}})$, where $F_{\text{tx}} = \frac{\theta_{\text{tx}}}{2\pi}$ and $F_{\text{rx}} = \frac{\theta_{\text{rx}}}{2\pi}$, respectively. Assuming that the main lobe of the typical mobile user's receiver is coinciding with that of its desired

[1]For the sake of brevity, I will drop the argument of $K_a(f_T)$ from this point onwards in the thesis.

TBS, its SINR the can be formulated as follows:

$$\begin{aligned}\text{SINR}_T &= \frac{G_T^{\text{tx}} G_T^{\text{rx}} \left(\frac{c}{4\pi f_T}\right)^2 P_T^{\text{tx}} \exp(-K_a d_0) d_0^{-2}}{N_T + I_T}, \\ &= \frac{\gamma_T \, P_T^{\text{tx}} \exp(-K_a d_0) d_0^{-2}}{N_T + I_T},\end{aligned} \tag{3.5}$$

where $I_T = \sum_{i \in \Phi_T \setminus 0} \gamma_T \; P_T^{\text{tx}} \; F {d_i}^{-2} \exp(-K_a \; d_i)$ is the cumulative interference at the mobile user, d_i is the distance of the that user to the i-th interfering TBS, F is the probability of alignment, and $\gamma_T = G_T^{\text{tx}} \; G_T^{\text{rx}} \; c^2/(4\pi f_T)^2$ considering negligible side-lobe gains. For clarity, negligible side lobe gains has been considered in the modeled interference; however, the proposed framework can be extended to include side-lobe gains in a straight-forward manner. The cumulative thermal and molecular absorption noise is:

$$N_T = N_0 + \; P_T^{\text{tx}} \gamma_T \; d_0^{-2} \; (1 - e^{-K_a \; d_0}) + \sum_{i \in \Phi_T \setminus 0} \gamma_T F \; P_T^{\text{tx}} \; d_i^{-2} (1 - \exp(-K_a \; d_i)).$$

The SINR from TBS can then be modeled as follows:

$$\text{SINR}_T = \frac{P_T^{\text{tx}} \; \gamma_T \; d_0^{-2} e^{-K_a \; d_0}}{N_0 + \; P_T^{\text{tx}} \gamma_T \; d_0^{-2} \; (1 - e^{-K_a \; d_0}) + \sum_{i \in \Phi_T \setminus 0} \; P_T^{\text{tx}} \gamma_T F \; d_i^{-2}}.$$

3.1.5 Methodology of Analysis

The methodology of analyzing the HO rate and mobility-aware coverage probability in a multi-band network can be summarized as follows:

- Derive the conditional probability density function (PDF) of the distance of a

mobile user if it is tagged to the TBS ($f_{r_T}(r_T)$) and RBS ($f_{r_R}(r_R)$) in a multi-band network.

- Derive the conditional HO probability of a typical user who is initially associated to TBS ($\mathbb{P}(H_T)$) and the HO probability of a mobile user who is initially associated to RBS ($\mathbb{P}(H_R)$).

- Using the association probabilities of the typical user to TBSs and RBSs, i.e., A_T and A_R, respectively, and conditional HO probabilities $\mathbb{P}(H_R)$ and $\mathbb{P}(H_T)$, derive the overall HO probability, i.e., $\mathbb{P}(H)$ of the typical user.

- Derive the Laplace Transform of the cumulative interference and molecular noise as well as the coverage probability of the typical user without mobility $\mathbb{C}$.

- Derive the coverage probability of the typical user with mobility $\mathbb{C}_M$.

3.2 Handoff Probability Analysis in a Hybrid RF-THz Network

In this section, we first develop HO criterion from TBS and derive the conditional HO probability from TBS, i.e., $\mathbb{P}(H_T)$. This conditional HO probability includes the HO probability from TBS to TBS (i.e., horizontal HO) and TBS to RBS (i.e., vertical HO). The conditional HO probability from TBS is defined as the probability of transferring an active mobile user from one tier of THz to another tier given that the mobile user is initially tagged to TBS. Later, I formulate and simplify the HO criterion from RBS and derive the HO probability from RBS, i.e, $\mathbb{P}(H_R)$, which comprises of the HO probability from RBS to RBS (horizontal HO) and RBS to TBS (vertical HO). Finally, develop the overall HO probability of the mobile user, which

is defined as:

$$\mathbb{P}(H) = A_R \mathbb{P}(H_R) + A_T \mathbb{P}(H_T), \tag{3.6}$$

where A_R and A_T denote the association probabilities of a user with RBS and TBS, respectively.

Remark: I have four possible events for HO of the typical user, such as, moving from RBS to RBS, moving from TBS to TBS, moving from RBS to TBS, and moving from TBS to RBS and each event has a specific probability. Each event depends on the previous association of the typical user, therefore, the process can possibly be perceived as a discrete time two-state Markov chain where the transition probabilities are given by the conditional HO probabilities. The Markov property holds as future state depends only on the current state, not on the events that occurred before it. Therefore, this framework is useful for predictive modelling and probabilistic forecasting.

From the relationship between the received powers of TBSs and RBSs, the association probability to TBS can be defined as follows:

$$\begin{aligned} A_T &= \mathbb{E}_{d_0}\left[\mathbb{P}\left(P_T^{\text{rx}} > P_R^{\text{rx}}\right)\right], \\ &= \mathbb{E}_{d_0}\left[\mathbb{P}\left(P_T^{\text{tx}}\gamma_T \frac{\exp\left(-K_a d_0\right)}{d_0^2} > P_R^{\text{tx}}\gamma_R r_0^{-\alpha}\right)\right], \\ &\overset{(a)}{=} \mathbb{E}_{d_0}\left[\exp\left(-\pi\lambda_R\left(Q d_0^2 \exp\left(K_a d_0\right)\right)^{\frac{2}{\alpha}}\right)\right], \end{aligned} \tag{3.7}$$

where from the null probability of PPP Φ_R and $Q = \frac{P_R^{\text{tx}}}{P_T^{\text{tx}}}\frac{\gamma_R}{\gamma_T}$, I get step (a) in Eq. (3.14). This null property stated the probability that no RBSs are closer to a user than the distance z, which is $\mathbb{P}\left(\rho \geq z\right) = \exp\left(-\pi\lambda_R z^2\right)$ for given a tier of RBSs with intensity λ_{R}. The PDFs of the distances between the typical user and the closest RBS and

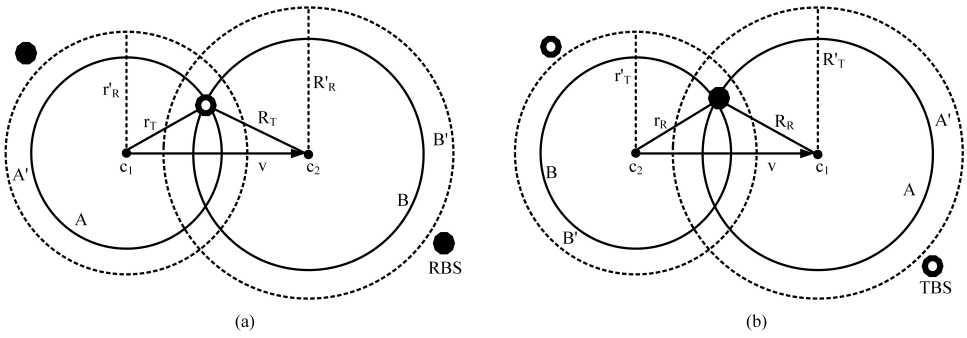

Figure 3.2: Illustration of different HO events, (a) HO from TBS: At c_1, a mobile user is initially associated with a TBS, where the distance between user and TBS is r_T. After moving at c_2, the distance becomes R_T. The virtual tiers are shown by the dotted lines, i.e., the equivalent distance of the TBS from c_1 and c_2 in RF tier is represented by r'_R and R'_R, respectively. (b) HO from RBS: At c_2, a mobile user is initially associated with a RBS, where the distance between user and RBS is r_R. After HO at c_1, the distance becomes R_R. The virtual tiers are shown by the dotted lines, i.e., the equivalent distance of the RBS from c_2 and c_1 is represented by r'_T and R'_T, respectively.

TBS are given as $f_{r_0}(r_0) = 2\pi\lambda_T r_0 \exp(-\pi\lambda_T r_0^2)$ and $f_{d_0}(d_0) = 2\pi\lambda_T d_0 \exp(-\pi\lambda_T d_0^2)$, respectively. Therefore, the association probability with TBS can be achieved by averaging over d_0.

$$A_T = \int_0^\infty \exp\left(-\pi\lambda_R Q^{\frac{2}{\alpha}}\, d_0^{\frac{4}{\alpha}} \exp\left(\frac{2K_a\, d_0}{\alpha}\right)\right) f_{d_0}(d_0) dd_0, \tag{3.8}$$

where $A_R = 1 - A_T$.

3.2.1 Handoff Probability Characterization from TBS

3.2.1.1 HO Criterion from TBS

Fig. 3.2(a) illustrates an outline of an user, who is initially tagged with a TBS at the position c_1. Let r_T is the distance between the user and TBS, given the user is

associated to a TBS in a hybrid RF-THz network.

Lemma 1. *The conditional PDF of the distance from a mobile user initially connected to TBS to the desired TBS is as follows:*

$$f_{r_T}(r_T) = \frac{2\pi\lambda_T\, r_T}{A_T} \cdot \exp\left(-\pi\lambda_T r_T^2 - \pi\lambda_R (r_T^2 Q)^{\frac{2}{\alpha}} \exp\left(\frac{2K_a r_T}{\alpha}\right)\right). \tag{3.9}$$

Proof. See **Appendix A**. □

The area A centered by c_1 with radius r_T. Assume that the user is performing a measurement and sends this measurement reports to the network while this user moves its position from c_1 to c_2. The new distance R_T denotes the distance between c_2 and TBS. The area B centered by c_2 with radius R_T. At position c_2, *the vertical HO event takes place when the maximum received power of RBS is greater than that of THz tier*, i.e., $P_T^{\text{rx}} < P_R^{\text{rx}}$, which results in the following:

$$r_R < \exp\left(\frac{K_a\, r_T}{\alpha}\right) \left(Q\, r_T^2\right)^{\frac{1}{\alpha}} \triangleq r'_R, \tag{3.10}$$

From Eq. (3.10), I define r'_R is the equivalent distance of r_T. That is, when $r_T > r_R > r'_R$, vertical HO will not occur because it violates Eq. (3.10).

3.2.1.2 Handoff Analysis

It has provided that the typical mobile user is originally tagged to THz tier, the conditional HO probability from TBS can be determined by averaging over r_T and θ as follows:

$$\mathbb{P}(H_T) = 1 - \mathbb{P}(\overline{H}_T) = 1 - \mathbb{E}_{r_T,\theta}[\mathbb{P}(\overline{H}_T | r_T, \theta)]. \tag{3.11}$$

To derive the no HO probability ($\mathbb{P}(\overline{H}_T)$) of a typical user who is associated to TBS, we replace the serving TBS by a virtual TBS in RF tier with distance r'_R away from the target mobile user. There will be no HO if no RBSs or TBSs are closer to the user then r'_R. In Fig. 3.2(a), the area A' centered at c_1 with radius r'_R. Here, the THz tier is the serving tier suggests all RBSs are found outside the area A'. Likewise, B' is the area centered at c_2 with radius R'_R, which is the corresponding distance of R_T. If RBSs are not remained within the area B', then initial TBS will remain the target BS even after the movement and therefore the chance of no HO will be higher.

Lemma 2. *Given a mobile user is initially associated with a TBS, the conditional probability of no HO from the serving TBS in a hybrid RF-THz network finds as follows:*

$$\begin{aligned}\mathbb{P}(\overline{H}_T) =& \frac{1}{\pi}\left(\int_{\theta=0}^{\frac{\pi}{2}}\int_{r_T=0}^{\infty} f_{r_T}(r_T)\exp\left(-\lambda_T S_T-\lambda_R S'_T\right)dr_T d\theta\right.\\ &+\int_{\theta=\frac{\pi}{2}}^{\pi}\int_{r_T=0}^{v\cos(\pi-\theta)} f_{r_T}(r_T)\exp\left(-\lambda_T C_T-\lambda_R C'_T\right)dr_T d\theta\\ &\left.+\int_{\theta=\frac{\pi}{2}}^{\pi}\int_{r_T=v\cos(\pi-\theta)}^{\infty} f_{r_T}(r_T)\exp\left(-\lambda_T S_T-\lambda_R S'_T\right)dr_T d\theta\right),\end{aligned}$$

where $S_T=|B|-|B\cap A|$, $S'_T=|B'|-|B'\cap A'|$, $C_T=R_T^2(\pi-\theta_1'^T)+r_T v\sin\theta-r_T^2(\pi-\theta)$, $C'_T=R_R'^2(\pi-\theta_3'^T)+r'_R\,v\,\sin\theta_2^T-r_R'^2(\pi-\theta_2^T)$, $\theta_1'^T=\theta-\pi+\sin^{-1}\left(\frac{v\sin\theta}{R_T}\right)$, $\theta_3'^T=\theta-\pi+\sin^{-1}\left(\frac{v\sin\theta}{R'_R}\right)$.

Proof. See **Appendix B**. □

In the following, as a special case of the aforementioned lemma, I have provided the HO probability of a mobile user for a stand-alone THz network.

Corollary 1. *The conditional HO probability in a single-tier THz network can be simplified as:*

$$\begin{aligned}\mathbb{P}(H_T) =& 1 - \frac{1}{\pi}\left(\int_{\theta=0}^{\frac{\pi}{2}}\int_{r_T=0}^{\infty} f_{d_0}(d_0)\exp\left(-\lambda_T S_T\right) dr_T d\theta\right. \\ &+ \int_{\theta=\frac{\pi}{2}}^{\pi}\int_{r_T=0}^{v\cos(\pi-\theta)} f_{d_0}(d_0)\exp\left(-\lambda_T C_T\right) dr_T d\theta \\ &\left.+ \int_{\theta=\frac{\pi}{2}}^{\pi}\int_{r_T=v\cos(\pi-\theta)}^{\infty} f_{d_0}(d_0)\exp\left(-\lambda_T S_T\right) dr_T d\theta\right).\end{aligned}$$

3.2.2 Handoff Probability Characterization from RBS

3.2.2.1 HO Criterion from RBS

Fig. 3.2(b) illustrates a situation where a typical mobile user is tagged with a given RBS at the position c_2. Let r_R be the distance between the mobile user and RBS, given the user is associated to the RBS in a multi-band network. The area centered by c_2 with radius r_R is denoted by B.

Lemma 3. *The PDF of the conditional distance r_R from a typical mobile user initially connected to RBS to desired RBS can be acquired as follows:*

$$f_{r_R}(r_R) = \frac{2\pi\lambda_R r_R}{A_R}\exp\left(-\pi\lambda_R r_R^2 - \pi\lambda_T\left(\frac{r_R^{\alpha}}{Q}\right)^{\frac{2}{2+\mu}}\right). \tag{3.12}$$

Proof. See **Appendix A**. □

Let R_R denotes the distance between c_1 and RBS. When user moves to c_1, the HO occurs if the maximum received power of TBS is greater than that of RF tier,

i.e., $P_R^{\text{rx}} < P_T^{\text{rx}}$, which results in the following:

$$r_T^2 \exp\left(K_a r_T\right) < (r_R)^{\alpha}(1/Q). \tag{3.13}$$

Note that the exponential term is a function of r_T; therefore, for the sake of tractability and to apply the equivalent distance approach, I approximate $r_T^{\mu} \approx \exp(K_a\, r_T)$ then, $r_T^2 \exp(K_a\, r_T) \approx (r_T)^{2+\mu}$. Subsequently, I have $r_T < [(r_R)^{\alpha}(1/Q)]^{\frac{1}{2+\mu}} \triangleq r'_T$, where μ is a correcting factor and r'_T specifies the virtual distance or equivalent distance of r_R. That is, the statement $r_R > r_T > r'_T$ is stopped to occurs the vertical HO between these two tiers due to the condition of $P_R^{\text{rx}} < P_T^{\text{rx}}$.

Choice of μ*:* To select μ appropriately, I calculate the probability of association of the typical mobile user to RBS by using the exact result of A_T in (3.8) and then equate it to the approximate association probability obtained as follows:

$$\begin{aligned}
\tilde{A}_R &= \mathbb{E}_{r_0}\left[\mathbb{P}\left(P_R^{\text{rx}} > P_T^{\text{rx}}\right)\right], \\
&= \mathbb{E}_{r_0}\left[\mathbb{P}\left(P_R \gamma_R r_0^{-\alpha} > P_T \gamma_T \frac{\exp\left(-K_a d_0\right)}{d_0^2}\right)\right], \\
&\approx \mathbb{E}_{r_0}\left[\mathbb{P}\left(P_R \gamma_R r_0^{-\alpha} > P_T \gamma_T d_0^{-2-\mu}\right)\right], \\
&\overset{(a)}{=} \mathbb{E}_{r_0}\left[\exp\left(-\pi \lambda_T \left(\frac{r_0^{\alpha}}{Q}\right)^{\frac{1}{2+\mu}}\right)\right], \\
&= \int_0^{\infty} \exp\left(-\pi \lambda_T \left(\frac{r_0^{\alpha}}{Q}\right)^{\frac{2}{2+\mu}}\right) f_{r_0}(r_0)\, dr_0.
\end{aligned} \tag{3.14}$$

Solving $A_R = \tilde{A}_R$ gives us the appropriate value of μ. Note that when the molecular absorption coefficient $K_a \to 0$, the value of $\mu \to 0$. In this case, the approximation becomes exact.

3.2.2.2 HO Analysis

It has shown the typical mobile user is originally associated to THz tier, the HO probability from RBS can be determined by taking the average over r_R and θ as follows:

$$\mathbb{P}(H_R) = 1 - \mathbb{P}(\overline{H}_R) = 1 - \mathbb{E}_{r_R,\theta}[\mathbb{P}(\overline{H}_R|r_R,\theta)]. \tag{3.15}$$

To derive the no HO probability ($\mathbb{P}[\bar{H}_R]$) of a mobile user who is tagged to RBS, I replace the serving RBS by a virtual RBS in THz tier, therefore, the new distance is r'_T away from the target mobile user. Fig. 3.2(b) shows the area B' centered at c_2 with radius r'_T. The fact that RF tier is acting as the serving tier to serve the mobile user indicates that all the other BSs of THz tier are situated outside B'. Here, the area A' with the radius R'_T, which is centered at c_1. The radius R'_T is the equivalent distance of R_R. If no TBSs are located in the area A', then initial RBS will remain the tagged BS even after movement of the user. There will be no HO if no RBSs or TBSs are closer then r'_R.

Lemma 4. *Given a mobile user is originally associated with a RBS, the probability of no HO from the serving RBS in a hybrid RF-THz network can be derived as follows:*

$$\begin{aligned}\mathbb{P}[\bar{H}_R] =& \frac{1}{\pi}\left(\int_{\theta=0}^{\frac{\pi}{2}}\int_{r_R=0}^{\infty} f_{r_R}(r_R)\exp\left(-\lambda_R S_R - \lambda_T S'_R\right) dr_R\, d\theta\right.\\ &+ \int_{\theta=\frac{\pi}{2}}^{\pi}\int_{r_R=0}^{v\cos(\pi-\theta)} f_{r_R}(r_R)\exp\left(-\lambda_R C_R - \lambda_T C'_R\right) dr_R\, d\theta\\ &\left.+ \int_{\theta=\frac{\pi}{2}}^{\pi}\int_{r_R=v\cos(\pi-\theta)}^{\infty} f_{r_R}(r_R)\exp\left(-\lambda_R S_R - \lambda_T S'_R\right) dr_R\, d\theta\right),\end{aligned}$$

where $S_R = |A| - |A \cap B|, S'_R = |A'| - |A' \cap B'|, C_R = R_R^2(\pi - \theta_1'^R) + r_R\, v\, sin\theta - r_R^2(\pi - \theta), C'_R = R_T'^2(\pi - \theta_3'^R) + r'_T\, v\, \sin\theta_2^R - r_T'^2(\pi - \theta_2^R), \theta_1'^R = \theta - \pi + \sin^{-1}\left(\frac{v\,\sin\theta}{R_R}\right), \theta_3'^R = \theta - \pi + \sin^{-1}\left(\frac{v\,\sin\theta}{R'_T}\right)$.

Proof. See **Appendix C**. □

3.2.3 Overall Handoff Probability

The HO probability of a mobile user in a hybrid RF-THz network finds as follows:

$$\mathbb{P}(H) = A_R\mathbb{P}(H_R) + A_T\mathbb{P}(H_T) = 1 - A_R\mathbb{P}(\bar{H}_R) + A_T\mathbb{P}(\bar{H}_T), \tag{3.16}$$

where A_R and A_T are given in (3.8). Likewise, $\mathbb{P}(\bar{H}_T)$ and $\mathbb{P}(\bar{H}_R)$ are given by **Lemma 2** and **Lemma 4**, respectively.

3.3 Coverage Probability With and Without Mobility

Coverage Probability is defined as the probability that a typical mobile user is able to achieve a predefined threshold SINR. In this section, first I characterize the conditional coverage probabilities from TBS and RBS, i.e., $\mathbb{C}_{\mathbb{T}}$ and $\mathbb{C}_R$, respectively. Then, the probability of coverage with and without mobility will be derived. Since a mobile user can connect to either RF or THz tier, the unconditional probability of coverage without mobility can demonstrate as follows:

$$\mathbb{C} = A_T\mathbb{C}_T + A_R\mathbb{C}_R, \tag{3.17}$$

where A_T and A_R are defined in Section III. Here, the TBSs and RBSs are distributed as different PPPs, therefore, the distance of a typical mobile user to its serving BS

depends on the associated tier. Afterwards, the PDF of the conditional distance of the typical mobile user to TBS and RBS can be given as in **Lemma 1** and **Lemma 3**, respectively.

3.3.1 Conditional Coverage Probability - THz

Conditional coverage probability is defined as the probability that a typical mobile user is able to achieve a predefined threshold SINR given the mobile user is tagged to TBS. The conditional rate coverage probability is defined as the probability of this user achieving a target data rate R_{th}. Using $R_{\text{th}} = W_T \log_2(1 + \text{SINR}_T)$ (where W_T is the bandwidth for THz transmission), the conditional rate coverage probability is given below:

$$\begin{aligned}\mathbb{C}_T &= \mathbb{P}\left(\text{SINR}_T > 2^{\frac{R_{\text{th}}}{W_T}} - 1\right) = \mathbb{P}\left(\text{SINR}_T > \tau_T\right), \\ &= \mathbb{P}\left(\frac{P_T^{\text{tx}} \gamma_T (r_{T,0})^{-2} \left((1+\tau_T)\exp\left(-K_a\, r_{T,0}\right) - \tau_T\right)}{N_0 + \sum_{i \epsilon \Phi \setminus 0} P_T^{\text{tx}} \gamma_T F(r_{T,i})^{-2}} > \tau_T\right). \end{aligned} \tag{3.18}$$

Taking

$$S(r_{T,0}) = (1+\tau_T) P_T^{\text{tx}} \gamma_T (r_{T,0})^{-2} \exp\left(-K_a r_{T,0}\right) - P_T^{\text{tx}} \gamma_T (r_{T,0})^{-2} \tau_T,$$

where, $I_T^{\text{agg}} = \sum_{i \epsilon \phi \setminus 0} P_T^{\text{tx}} \gamma_T F(r_{T,i})^{-2}$ is the cumulative interference at the typical mobile user and applying Gil-Pelaez inversion theorem, Eq. (3.18) can be rewritten

as follows:

$$\begin{aligned}\mathbb{C}_T &= \mathbb{P}\left(\frac{S(r_{T,0})}{N_0 + I_T^{\text{agg}}} > \tau_T\right), \\ &= \mathbb{P}\left(S(r_{T,0}) > \tau_T N_0 + \tau_T I_T^{\text{agg}}\right), \\ &= \mathbb{E}_{r_{T,0}}\left[\frac{1}{2} - \frac{1}{\pi}\int_0^\infty \frac{\text{Im}[\phi_{\Omega|r_{T,0}}(\omega)\exp\left(j\omega\tau_T N_0\right)]}{\omega} d\omega\right], \end{aligned} \tag{3.19}$$

where $\text{Im}(\cdot)$ denotes the imaginary operator, $\Omega = S(r_{T,0}) - \tau_T I_{\text{agg}}^T$, and $\phi_\Omega(\omega) = \mathbb{E}[\exp\left(-j\omega\Omega\right)]$ denotes the characteristic fuction (CF) of Ω can be stated as follows:

$$\phi_{\Omega|r_{T,0}}(\omega) = \exp\left(-j\omega S(r_{T,0})\right)\mathcal{L}_{I_T^{\text{agg}}|r_{T,0}}(-j\omega\tau_T). \tag{3.20}$$

where $\mathcal{L}_{I_{\text{agg}}^T|r_T}$ is the Laplace Transform of the cumulative interference conditioned on $r_{T,0}$ and is derived in the following Lemma.

Lemma 5. *The LT of the cumulative interference can be given as follows:*

$$\mathcal{L}_{I_T^{\text{agg}}}(s) = \exp\left(2\pi\lambda_T \sum_{l=1}^{\infty} \frac{\left(-sF\gamma_T P_{\text{T}}^{\text{tx}}\right)^l}{(2l-2)\,l!} \cdot \frac{1}{(r_{T,0})^{2l-2}}\right),$$

where $F = G_{\max}^{\text{tx}} G_{\max}^{\text{rx}}/4\pi^2$ is the probability of main-lobe alignment of the interferers and the typical user and given negligible side lobe gains.

Proof. Starting from the definition of LT, I have:

$$\begin{aligned}
\mathcal{L}_{I_T^{\text{agg}}}(s) &= \mathbb{E}_{\Phi_T}\left[\exp\left(-sI_T^{\text{agg}}\right)\right] = \mathbb{E}_{\Phi_T}\left[\exp\left(-sF\sum_{i\in\Phi_T\setminus 0} P_T^{\text{tx}}\gamma_T(r_{T,i})^{-2}\right)\right], \\
&= \mathbb{E}_{\Phi_T}\left[\prod_{i\in\Phi_T\setminus 0}\exp\left(-sFP_T^{\text{tx}}\gamma_T(r_{T,i})^{-2}\right)\right], \\
&\overset{(a)}{=} \exp\left(-2\pi\lambda_T\int_{r_{T,0}}^{\infty} r_{T,i}\left(1-\exp\left(-sF\gamma_T P_{\text{T}}^{\text{tx}}(r_{T,i})^{-2}\right)\right)dr_{T,i}\right), \\
&\overset{(b)}{=} \exp\left(2\pi\lambda_T\int_{r_{T,0}}^{\infty}\sum_{l=1}^{\infty}\frac{\left(-sF\gamma_T P_{\text{T}}^{\text{tx}}\right)^l}{(r_{T,i})^{2l-1}l!}dr_{T,i}\right), \\
&\overset{(c)}{=} \exp\left(2\pi\lambda_T\sum_{l=1}^{\infty}\frac{\left(-sF\gamma_T P_{\text{T}}^{\text{tx}}\right)^l}{(2l-2)\,l!}\,\frac{1}{(r_{T,0})^{2l-2}}\right),
\end{aligned}$$

where with the help of the probability generating functional (**PGFL**), step (a) has obtained by $f(x) = \exp\left(-sP_T h\left(r_{T,i}\right)\right)$ (b) is obtained by using $\exp\left(-x\right) = \sum_{i=0}^{\infty}(-1)^i\frac{x^i}{i!}$ ([51], Eq. 1.211). Since the mobile user has maintained a distance $r_{T,0}$ from its tagged TBS, all interferers are beyond this distance $r_{T,0}$, which is also the lower limit of the integral.

Remark: LT expression for aggregate interference is needed to derive coverage probability using Gil-Pelaez inversion. Gil-Pelaez inversion can calculate the CDF or complementary cumulative density function (CCDF) of any random variable by using the CF of that random variable. Here, the random variable is Ω and I am using its CF of Ω in Gil-Pelaez inversion to calculate the coverage. The CF of Ω can only be obtained using the LT of the aggregate interference as shown in Eq.(3.20).

□

3.3.2 Conditional Coverage Probability - RF

The conditional probability of coverage of the mobile user, which is tagged to RBS can be derived in an interference limited regime as follows [9]:

$$\begin{aligned}\mathbb{C}_R &= \mathbb{P}\left(\frac{P_R^{tx}\gamma_R H}{(r_{R,0})^{\alpha} I_R^{\text{agg}}} > \tau_R\right), \\ &= \mathbb{P}\left(H > \tau_R (P_R^{tx})^{-1}\gamma_R^{-1}(r_{R,0})^{\alpha} I_R^{\text{agg}}\right), \\ &= \mathbb{E}\left[\exp(-\tau_R (P_R^{tx})^{-1}\gamma_R^{-1}(r_{R,0})^{\alpha} I_R^{\text{agg}})\right], \\ &= \int_0^{\infty} \mathcal{L}_{I_R^{\text{agg}}}\left(\tau_R (P_R^{tx})^{-1}\gamma_R^{-1}(r_{R,0})^{\alpha}\right) f_{r_{R,0}}(r_{R,0}) dr_R, \end{aligned} \tag{3.21}$$

where $\mathcal{L}_{I_R^{\text{agg}}}\left(\tau_R (P_R^{tx})^{-1}\gamma_R^{-1}(r_{R,0})^{\alpha}\right) = \exp\left(-\pi (r_{R,0})^2 \lambda_R \mathcal{Y}(\tau_R, \alpha)\right)$. Here, $\mathcal{Y}(\tau_R, \alpha) = \frac{2\tau_R}{\alpha - 2} {}_2F_1[1, 1 - \frac{2}{\alpha}; 2 - \frac{2}{\alpha}; -\tau_R]$, and ${}_2F_1[\cdot]$ is the Gauss's Hypergeometric function.

3.3.3 Coverage Probability With and Without Mobility

The overall coverage probability without mobility in a hybrid RF-THz network is given by substituting the conditional coverage probability results given in (3.23) and (3.21) into (3.17). The overall coverage probability with mobility is a function of HO probability. The coverage degrades with the higher HO probability, service delays, and dropped calls. The overall coverage with mobility can then be modeled as follows [15]:

$$\mathbb{C}_M = \mathbb{C}\left(1 - \eta\, \mathbb{P}(H)\right), \tag{3.22}$$

where η is the system's sensitivity to the HO and as η increases the probability of connection failure increases due to HO. For $\eta = 0$, the mobility has no impact on the coverage probability, whereas for $\eta = 1$, this probability depends solely on HO

probability. That is, as $\mathbb{P}(H) = 1$, the coverage probability becomes zero. Note that $\mathbb{C}$ is the total coverage probability of a typical mobile user in a hybrid RF-THz network without mobility given by (3.17) and $\mathbb{P}(H)$ is the overall HO probability for that mobile user in a hybrid RF-THz network given by (3.16).

Remark: As a special case, the overall coverage probability without mobility in a stand-alone THz network can be given simply by averaging (3.23) over d_0 instead of $r_{T,0}$. Furthermore, in the case of noise-limited regime, i.e., when the interference is negligible, the coverage probability in a stand-alone THz network can be simplified as shown in the following.

Corollary 2. *In the noise-limited regime (in scenarios where the intensity of TBSs is low), the coverage probability of a typical user can be simplified as follows:*

$$\begin{aligned}\mathbb{C}_T &= \mathbb{P}\left(S(r_{T,0}) > \tau_T N_0\right), \\ &\overset{(a)}{=} \mathbb{E}_{r_{T,0}}\left[\frac{1}{2} - \frac{1}{\pi}\int_0^\infty \frac{\mathrm{Im}[\exp\left(-j\omega(S(r_{T,0}) - \tau_T N_0)\right]}{\omega} d\omega\right], \\ &= \frac{1}{2} + \frac{1}{\pi}\mathbb{E}_{r_{T,0}}[\int_0^\infty \frac{\sin\left(\omega(S(r_{T,0}) - \tau_T N_0\right)}{\omega} d\omega], \end{aligned} \tag{3.23}$$

where (a) follows from Euler's identity, i.e., $e^{-j\theta} = \cos\theta - j\sin\theta$.

3.4 Numerical Results and Discussions

In this section, the derived expressions has been validated by Monte-Carlo simulations with the consideration of a hybrid RF-THz network. To validate the mathematical expressions in my research problem, Monte-Carlo simulations provide a platform for simulating the key performance metrics like HO probability, association probability,

and coverage probability by calculating statistical averages over several random variables (e.g., locations of BSs, location of users from BSs in polar coordinate system, and channel fading). In particular, I am averaging the whole process over 10,000 snapshots in order to generate my simulation results. These simulation results are then used to validate my analytical expressions to confirm their accuracy. The results in this thesis extract useful insights related to the probability of coverage of a moving user within a hybrid RF-THz network considering the impact of molecular noise in THz transmission, intensity of TBSs, desired rate requirement, and velocity of a user.

3.4.1 Simulation Parameters

Unless stated otherwise, the users and BSs are located within a radius of 500 m circular region. The transmit power from TBS is 0.2 W and intensity of TBS is 0.0001 BSs/m^2. The transmit and receive antenna gains (i.e., G_T^{tx} and G_T^{rx}) of TBSs are considered as 25 dB. The THz carrier frequency is 1 THz. Desired target rate is 1 Gbps and THz transmission bandwidth is taken as 0.5 GHz. On the other hand, the transmit power from RBS is 2 W, where its transmission frequency is 2 GHz and transmission bandwidth is 40 MHz. Here, the exponent of path loss α is 4, and the intensity of RBSs is 0.00001 BSs/m^2.

3.4.2 Results and Discussions

Fig. 3.3 depicts the HO probability calculated for a typical mobile user who is tagged to TBS as a function of its velocity and intensity of the RBSs and TBSs. I compare the accuracy of my numerical results with the corresponding simulation results and note that the analytical results match perfectly with the Monte-Carlo simulations.

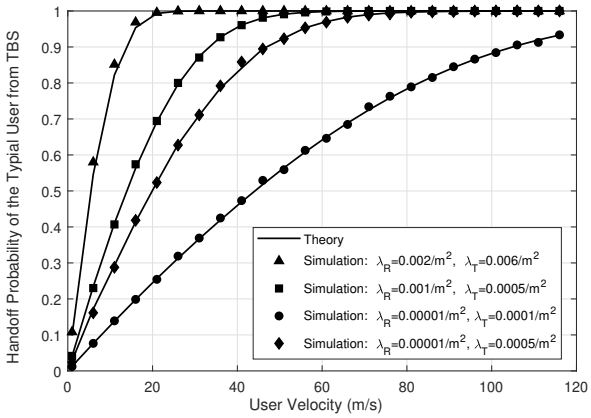

Figure 3.3: HO probability of a typical user from TBS as a function of the velocity and intensity of TBSs, $K_a = 0.01\text{m}^{-1}$.

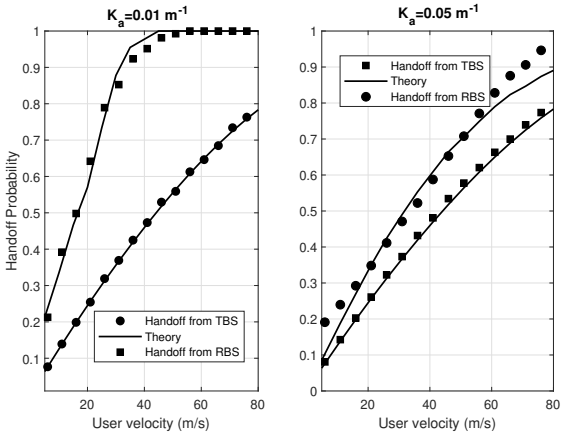

Figure 3.4: HO probability of a typical user as a function of the velocity and molecular absorption in a hybrid RF-THz network, $\lambda_R = 0.00001$ per m^2 and $\lambda_T = 0.0001$ per m^2.

The molecular absorption coefficient is set as $K_a = 0.01\text{m}^{-1}$. I observe that the HO probability increases with the increase in the number of RBSs; however, the increase is much more significant with the increase in TBSs. That is, I note that increasing λ_T from 0.0001 to 0.0005 per m^2 [i.e., almost 5 times] at $\lambda_R = 0.00001$ per m^2 increases the HO probability much more compared to the case when λ_R increases from 0.00001

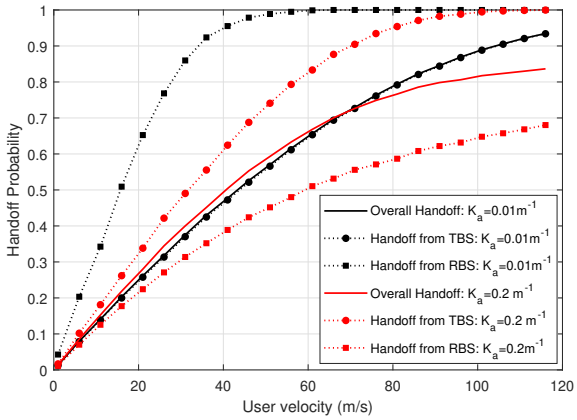

Figure 3.5: Overall HO probability of a typical user as a function of the velocity and molecular absorption in a hybrid RF-THz network, $\lambda_R = 0.00001$ per m^2 and $\lambda_T = 0.0001$ per m^2.

to 0.001 per m^2 [i.e., almost 100 times] at $\lambda_T = 0.0005$ per m^2. This signifies the impact of severe molecular absorption and small coverage zones on the connectivity of mobile users transmitting in a hybrid RF-THz network.

Fig. 3.4 depicts the impact of user's velocity on the conditional HO probability from TBS and conditional HO probability from RBS considering two different absorption coefficients, i.e., $K_a = 0.01$ m^{-1} and $K_a = 0.05$ m^{-1}. For lower values of K_a, the HO probability is much higher if the user was initially associated to RBS compared to the case if the user was initially connected to TBS. Also, in this case, the HO probability increases much rapidly with the increase in velocity. The reason is the high-received signal power from TBS compared to RBS generates more BS-switching. Conversely, for higher molecular absorption (i.e., $K_a = 0.05$ m^{-1}), I note an opposite trend. That is, the HO probability is much higher if the user was initially associated to TBS compared to the case when the user was initially connected to RBS. The reason is the severe molecular absorption which degrades the received signal from

TBS and favors shifting users from TBS to RBS. Finally, it can be observed that as the molecular absorption coefficient $K_a \to 0$, the analytical results matches perfectly with the Monte-Carlo simulations. Conversely, for of $K_a = 0.05$, the impact of approximation can be observed clearly. Note that the HO from TBS is exact and the approximation is only in the HO from RBS.

Fig. 3.5 has been plotted by keeping the intensity of BSs fixed (i.e., $\lambda_R = 0.00001$ per m^2 and $\lambda_T = 0.0001$ per m^2) and tracking the variation of the HO probability from TBS (H_T), HO probability from RBS (H_R), and overall HO probability of a typical mobile user with different molecular absorption coefficients. In the figure, the black curves consider $K_a = 0.01$ m^{-1}, whereas the red curves assume $K_a = 0.2$ m^{-1}. It can be observed that for low molecular absorption coefficient, the HO probability from RBS is much higher. The reason is that the lower molecular absorption favours association with TBS due to higher received powers. Conversely, when the molecular absorption coefficient is high, the HO probability from TBS is much higher, i.e., for the user who is initially associated with TBS. The reason is that the impact of molecular absorption is devastating; therefore, the criterion favours association with RBS. Nevertheless, the overall HO probability remains nearly the same which highlights the significance of computing and extracting insights from (H_T) and (H_R) separately.

Fig. 3.6 demonstrates the impact of thermal and molecular absorption noise on the coverage probability of a static user for two different molecular absorption coefficients, K_a, as a function of user's desired data rate. My analytical results match well with the simulation results. As expected, the coverage probability decreases with the increase in the target data rate. Furthermore, the impact of molecular noise is

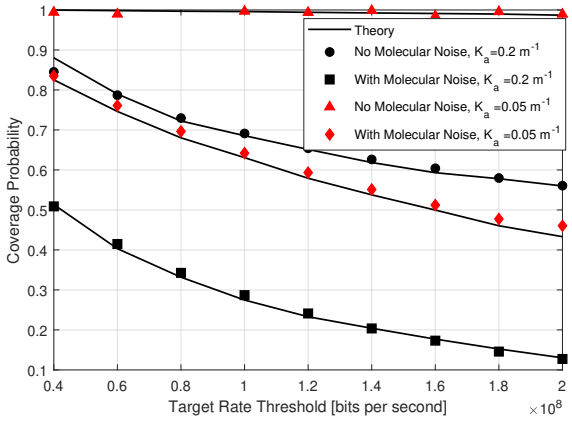

Figure 3.6: Coverage probability of a typical user as a function of the target rate threshold (in bps), $\lambda_R = 0.00001$ per m^2 and $\lambda_T = 0.0001$ per m^2.

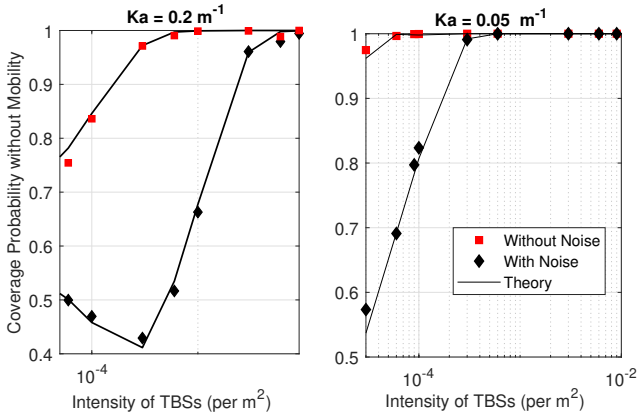

Figure 3.7: Coverage probability of a typical user as a function of the intensity of TBSs and molecular absorption in a hybrid RF-THz network, $K_a = 0.05\text{m}^{-1}$ and $K_a = 0.01\text{m}^{-1}$.

devastating and substantiate that ignoring molecular noise from the analytical results (as is done in [9]) can lead to over-optimistic results. Furthermore, with the increase in molecular absorption, the coverage probability degrades considerably.

Fig. 3.7 depicts the coverage probability with and without molecular noise as a function of the intensity of TBSs. The intensity of RBSs kept constant, and the

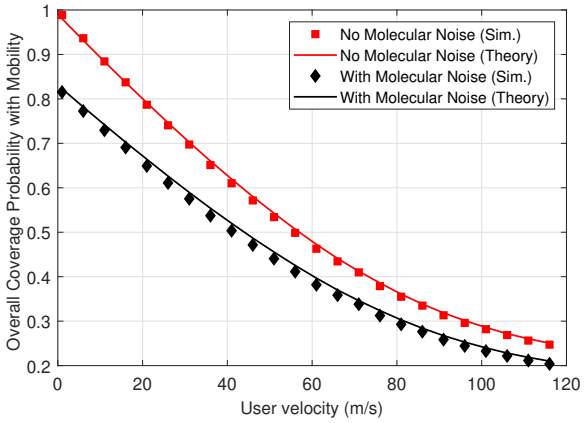

Figure 3.8: Mobility-aware coverage probability with a relation of a function of the user's velocity with and without molecular absorption, $\mu = 0.82$, $K_a = 0.05\text{m}^{-1}$.

user is static, however, the coverage probability is observed for two different values of molecular absorption coefficient. The analytical results corroborate with the simulation results. This figure also confirms that the molecular noise significantly degrades the coverage probability compared to the case when there is no molecular noise [9]. Furthermore, in general, the increase in intensity of TBSs increases coverage due to the shortening of distance from the nearest TBS. Interestingly, when molecular absorption is high, increasing the intensity first deteriorates the coverage probability (due to increased interference); and afterwards escalate due to improved signal quality which is mainly due to shorter distance from the associated TBS.

Fig. 3.8, demonstrate the overall coverage probability with mobility from Eq. (3.22) as a function of user's velocity. Numerical values from simulation results validate the accuracy of the theoretical results. This figure confirms the overall coverage probability reduces with the increase in velocity and demonstrates the gap between the results with molecular noise and without molecular noise in [9].

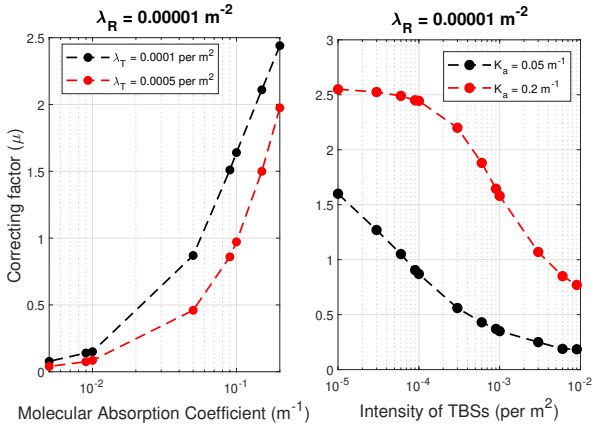

Figure 3.9: The correction factor as a function of the intensity of the TBSs and molecular absorption.

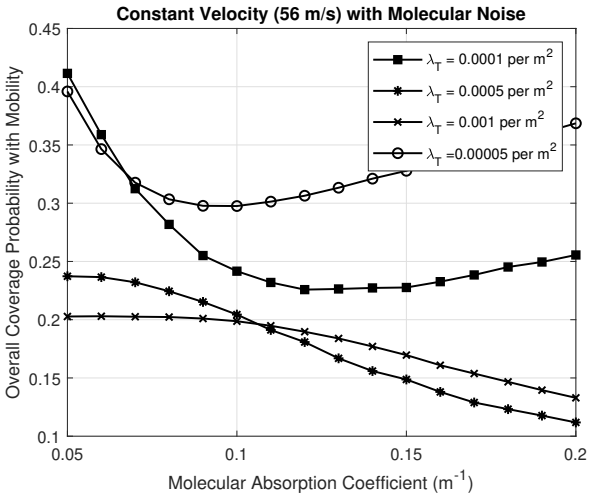

Figure 3.10: Overall coverage probability of a typical user with mobility as a function of the molecular absorption coefficient considering molecular noise and a constant user's velocity.

Fig. 3.9 illustrates the correcting factor (μ) as a function of the molecular absorption coefficient (K_a) and intensity of TBSs considering a fixed intensity of RBSs. The figure shows that the correcting factor gradually increases with the increasing value of molecular absorption coefficient. On the other hand, the figure demonstrates that the correcting factor gradually decreases with the increasing intensities of TBSs.

Fig. 3.10 depicts the overall coverage probability with mobility as a function of the molecular absorption coefficient and intensity of TBSs. I consider the user is moving with a constant velocity (i.e., 56 m/s). The higher intensity of TBSs ($\lambda_T = 0.001$ per m^2 and $\lambda_T = 0.0005$ per m^2) results in a much denser THz network and the connected TBSs are likely to be much closer to the moving user. Therefore, increasing the value of molecular absorption simply degrades the probability of coverage. This degradation is due to the reduction in signal strength. However, a more interesting observation can be noted from the cases when the intensity of TBSs are $\lambda_T = 0.0001$ per m^2 and $\lambda_T = 0.00005$ per m^2. That is, the overall coverage probability first reduces due to the signal degradation as a function of the molecular absorption. However, the coverage starts increasing again at some point and the reason is the reduction in interference with the increase of molecular absorption coefficient. Surprisingly, the benefits of interference reduction due to increasing molecular absorption dominates the drawback of signal degradation for a reasonable intensity of TBSs. This trend is opposite to what observed for much denser THz network.

3.5 Summary

In this chapter, I characterize the overall HO rate of a hybrid RF-THz network, considering the maximum received signal power association criterion. I analyze the

exact coverage probability of a typical user in the THz networks considering the impact of thermal and molecular absorption noise. The impact of user mobility or HO probability on overall coverage probability is shown at the end of this chapter. Finally, the derived expressions have been validated by comparing the results from theoretical with simulation results and summarized the outcomes based on the results.

Chapter 4

Conclusions and Future Directions

4.1 Conclusion

In this thesis, I provided a comprehensive stochastic geometry framework to describe the overall performance of a mobile user in a two-tier hybrid RF-THz network. Using stochastic geometry tools, I developed a tractable framework to calculate the HO rate and its impact on the probability of coverage of a typical mobile user in a hybrid RF-THz network. My framework is unified to capture different network configurations such as THz-only, RF-only, and hybrid RF-THz networks. I derived novel coverage probability expressions considering molecular noise in THz transmissions and derived the coverage probability with mobility. I validated the accuracy of derived expressions using Monte-Carlo simulations. The numerical results depict that the probability of HO in THz network is of much more significance than in conventional RF network, especially for lower molecular absorption coefficients. Therefore, mobility-aware performance frameworks are of immediate relevance. Also, the results demonstrated that the benefits of interference reduction due to increasing molecular absorption can dominate compared to the signal degradation at reasonable intensity of TBSs. This

is favourable news for upcoming 6G networks. Furthermore, the results revealed that ignoring molecular absorption and mobility can lead to significantly over-optimistic results, especially in high frequency THz networks.

4.2 Future Work

The outcomes explored in this thesis can be extended in the following ways:

4.2.1 Machine Learning for HO Prediction

Machine learning (ML) is known to solve different problems in the paradigm of wireless communications, such as, channel state estimation and precoding, topology formation and management, advance traffic control and cache management, fault estimation and recognition along with HO management. The proposed framework can be modeled as a two-state Markov chain which can be used for probabilistic forecasting of HOs for the typical user. This model can be used at each user's end in a distributed manner to predict HOs and this information can be send to a centralized controller to predict the network resource allocations and network congestion. Having such predictions at the network controller can help minimizing unnecessary HOs and keeping the reliability intact for existing 5G and beyond 5G systems.

4.2.2 Mobility-Aware Spectrum Selection

Different band of frequencies (e.g., RF and THz bands) are not applicable to serve different kind of users. Therefore, a mobility-aware network selection or user association methodology would be useful for different kinds of users, which is depending on the user's criterion, such as, mobility. Certain category users are using a dedicated band

of frequencies and are not allowed to use other band of frequencies. This strategy will expressively decrease unnecessary HO and ensure a reliable communication link.

4.2.3 Energy Efficient Deployment of Multi-band BSs

To increase the coverage, it is crucial to deploy BSs densely with massive antennas. However, the dense deployment of BSs and antennas consume huge power thus not energy efficient. One possible solution could be integrated BSs transmitting on a variety of transmission frequencies with optimized deployment of BSs [52–54]. Another solution would be to employ efficient power control [55]. This power control and antenna selection algorithm can consider maximizing the mobility-aware probability.

Bibliography

[1] D. Safer, F. Lalani, A. Alexa, T. Wedekamm, S. Dhar, and T. Rao, "Fuel for innovation: Canada's path in the race to 5G," 2018. [Online]. Available: https://www.5gcc.ca/

[2] A. Yastrebova, R. Kirichek, Y. Koucheryavy, A. Borodin, and A. Koucheryavy, "Future networks 2030: architecture & requirements," in *2018 10th International Congress on Ultra Modern TeleCommun. and Control Systems and Workshops (ICUMT)*, 2018, pp. 1–8.

[3] A. Dogra, R. K. Jha, and S. Jain, "A survey on beyond 5G network with the advent of 6G: Architecture and emerging technologies," *IEEE Access*, pp. 1–1, 2020.

[4] L. Zhang, Y. Liang, and D. Niyato, "6G visions: Mobile ultra-broadband, super internet-of-things, and artificial intelligence," *China Commun.*, vol. 16, no. 8, pp. 1–14, 2019.

[5] J. Kokkoniemi, J. Lehtomäki, and M. Juntti, "A discussion on molecular absorption noise in the terahertz band," *Nano Commun. Networks*, vol. 8, no. 1878-7789, pp. 35–45, 2016.

[6] H. Ibrahim, H. Tabassum, and U. T. Nguyen, "The meta distributions of the SIR/SNR and data rate in coexisting sub-6GHz and millimeter-wave cellular networks," *IEEE Open Journal of the Commun. Society*, vol. 1, pp. 1213–1229, 2020.

[7] H. Tabassum and E. Hossain, "Coverage and rate analysis for co-existing RF/VLC downlink cellular networks," *IEEE Trans. on Wireless Commun.*, vol. 17, no. 4, pp. 2588–2601, 2017.

[8] H. Elgala, M.-S. Alouini, H. Haas, M. Rahaim, H. Tabassum, and T. Watanabe, "Introduction to the special section on coexisting radio and optical wireless deployments (CROWD)," *IEEE Trans. on Cognitive Commun. and Networking*, vol. 5, no. 4, pp. 1178–1181, 2019.

[9] J. Sayehvand and H. Tabassum, "Interference and coverage analysis in coexisting RF and dense terahertz wireless networks," *IEEE Wireless Commun. Letters*, vol. 9, no. 10, pp. 1738–1742, 2020.

[10] N. Lu, N. Cheng, N. Zhang, X. Shen, and J. W. Mark, "Connected vehicles: Solutions and challenges," *IEEE Internet of Things Journal*, vol. 1, no. 4, pp. 289–299, 2014.

[11] P. Fan, J. Zhao, and C. I., "5G high mobility wireless communications: Challenges and solutions," *China Commun.*, vol. 13, no. Supplement2, pp. 1–13, 2016.

[12] J. Wu and P. Fan, "A survey on high mobility wireless communications: Challenges, opportunities and solutions," *IEEE Access*, vol. 4, pp. 450–476, 2016.

[13] S. Sadr and R. S. Adve, "Handoff rate and coverage analysis in multi-tier heterogeneous networks," *IEEE Trans. on Wireless Commun.*, vol. 14, no. 5, pp. 2626–2638, 2015.

[14] S. Hsueh and K. Liu, "An equivalent analysis for handoff probability in heterogeneous cellular networks," *IEEE Commun. Letters*, vol. 21, no. 6, pp. 1405–1408, 2017.

[15] C. Chen and X. Zhao, "Mobility-aware access strategy in multi-user hetnets," *IEEE Wireless Commun. Letters*, vol. 9, no. 7, pp. 1004–1008, 2020.

[16] N. Hassan, M. T. Hossan, and H. Tabassum, "User association in coexisting RF and terahertz networks in 6G," *IEEE Canadian Conference of Electrical and Computer Engineering*, 2020.

[17] A.-A. A. Boulogeorgos, E. N. Papasotiriou, and A. Alexiou, "Analytical performance assessment of THz wireless systems," *IEEE Access*, vol. 7, pp. 11 436–11 453, 2019.

[18] J. Kokkoniemi, J. Lehtomäki, and M. Juntti, "Stochastic geometry analysis for mean interference power and outage probability in THz networks," *IEEE Trans. on Wireless Commun.*, vol. 16, no. 5, pp. 3017–3028, 2017.

[19] C. Chaccour, R. Amer, B. Zhou, and W. Saad, "On the reliability of wireless virtual reality at terahertz (THz) frequencies," in *10th IFIP Int. Conf. on New Technologies, Mobility and Security (NTMS)*, 2019.

[20] X. Yao, C. Wang, and C. Qi, "Interference and coverage analysis for indoor THz communications with beamforming antennas," in *IEEE/CIC International*

Conference on Commun. Workshops in China (ICCC Workshops), 2019, pp. 147–152.

[21] A. Shafie, N. Yang, and C. Han, "Multi-connectivity for indoor terahertz communication with self and dynamic blockage," in *ICC 2020 - 2020 IEEE International Conference on Communications (ICC)*, 2020, pp. 1–7.

[22] X.-W. Yao, C.-C. Wang, and C.-F. Qi, "Interference and coverage analysis for indoor THz communications with beamforming antennas," in *IEEE/CIC Int. conf. on Commun. wkshps. in China*, 2019.

[23] K. Ntontin and C. Verikoukis, "Toward the performance enhancement of microwave cellular networks through THz links," *IEEE Trans. on Vehicular Technology*, vol. 66, no. 7, pp. 5635–5646, 2016.

[24] X. Lin, R. K. Ganti, P. J. Fleming, and J. G. Andrews, "Towards understanding the fundamentals of mobility in cellular networks," *IEEE Trans. on Wireless Commun.*, vol. 12, no. 4, pp. 1686–1698, 2013.

[25] H. Ibrahim, H. ElSawy, U. T. Nguyen, and M. Alouini, "Mobility-aware modeling and analysis of dense cellular networks with C -plane/ U -plane split architecture," *IEEE Trans. on Commun.*, vol. 64, no. 11, pp. 4879–4894, 2016.

[26] H. Tabassum, M. Salehi, and E. Hossain, "Fundamentals of mobility-aware performance characterization of cellular networks: A tutorial," *IEEE Commun. Surveys & Tutorials*, vol. 21, no. 3, pp. 2288–2308, 2019.

[27] C. Choi and F. Baccelli, "An analytical framework for coverage in cellular networks leveraging vehicles," *IEEE Trans. on Commun.*, vol. 66, no. 10, pp. 4950–4964, 2018.

[28] V. V. Chetlur and H. S. Dhillon, "Coverage analysis of a vehicular network modeled as cox process driven by poisson line process," *IEEE Trans. on Wireless Commun.*, vol. 17, no. 7, pp. 4401–4416, 2018.

[29] ——, "Success probability and area spectral efficiency of a VANET modeled as a cox process," *IEEE Wireless Commun. Letters*, vol. 7, no. 5, pp. 856–859, 2018.

[30] S. Aditya, H. S. Dhillon, A. F. Molisch, and H. Behairy, "Asymptotic blind-spot analysis of localization networks under correlated blocking using a poisson line process," *IEEE Wireless Commun. Letters*, vol. 6, no. 5, pp. 654–657, 2017.

[31] C. Choi and F. Baccelli, "Poisson cox point processes for vehicular networks," *IEEE Trans. on Vehicular Technology*, vol. 67, no. 10, pp. 10 160–10 165, 2018.

[32] V. V. Chetlur and H. S. Dhillon, "Coverage and rate analysis of downlink cellular vehicle-to-everything (C-V2X) communication," *IEEE Trans. on Wireless Commun.*, vol. 19, no. 3, pp. 1738–1753, 2020.

[33] C. Choi and F. Baccelli, "Spatial and temporal analysis of direct communications from static devices to mobile vehicles," *IEEE Trans. on Wireless Commun.*, vol. 18, no. 11, pp. 5128–5140, 2019.

[34] H. A. Ammar, A. K. Ajami, and H. Artail, "A poisson line process-based framework for determining the needed RSU density and relaying Hops in vehicular

networks," *IEEE Trans. on Wireless Commun.*, vol. 19, no. 10, pp. 6643–6659, 2020.

[35] Y. Sun, Z. Ding, and X. Dai, "On the outage performance of network NOMA (N-NOMA) modeled by poisson line cox point process," 2019.

[36] A. A. Boulogeorgos and A. Alexiou, "Error analysis of mixed THz-RF wireless systems," *IEEE Commun. Letters*, vol. 24, no. 2, pp. 277–281, 2020.

[37] A. S. Cacciapuoti, R. Subramanian, K. R. Chowdhury, and M. Caleffi, "Software-defined network controlled switching between millimeter wave and terahertz small cells," *arXiv preprint arXiv:1702.02775*, 2017.

[38] V. Petrov, J. Kokkoniemi, D. Moltchanov, J. Lehtomäki, M. Juntti, and Y. Koucheryavy, "The impact of interference from the side lanes on mmWave/THz band V2V communication systems with directional antennas," *IEEE Trans. on Vehicular Technology*, vol. 67, no. 6, pp. 5028–5041, 2018.

[39] H. S. Dhillon, R. K. Ganti, and J. G. Andrews, "A tractable framework for coverage and outage in heterogeneous cellular networks," in *2011 Information Theory and Applications Workshop*. IEEE, 2011, pp. 1–6.

[40] H. S. Dhillon, R. K. Ganti, F. Baccelli, and J. G. Andrews, "Modeling and analysis of K-tier downlink heterogeneous cellular networks," *IEEE Journal on Sel. Areas in Commun.*, vol. 30, no. 3, pp. 550–560, 2012.

[41] H.-S. Jo, Y. J. Sang, P. Xia, and J. G. Andrews, "Heterogeneous cellular networks with flexible cell association: A comprehensive downlink SINR analysis," *IEEE Trans. on Wireless Commun.*, vol. 11, no. 10, pp. 3484–3495, 2012.

[42] Q. Ye, B. Rong, Y. Chen, M. Al-Shalash, C. Caramanis, and J. G. Andrews, "User association for load balancing in heterogeneous cellular networks," *IEEE Trans. on Wireless Commun.*, vol. 12, no. 6, pp. 2706–2716, Jun. 2013.

[43] J. Rubio, A. Pascual-Iserte, J. del Olmo, and J. Vidal, "User association strategies in HetNets leading to rate balancing under energy constraints," *EURASIP Journal on Wireless Commun. and Networking*, vol. 2017, no. 1, p. 204, 2017.

[44] Q. Ye, O. Y. Bursalioglu, H. C. Papadopoulos, C. Caramanis, and J. G. Andrews, "User association and interference management in massive MIMO HetNets," *IEEE Trans. on Commun.*, vol. 64, no. 5, pp. 2049–2065, 2016.

[45] A. Zappone, L. Sanguinetti, and M. Debbah, "User association and load balancing for massive MIMO through deep learning," in *52nd Asilomar Conference on Signals, Systems, and Computers*. IEEE, 2018, pp. 1262–1266.

[46] S. Mumtaz, J. M. Jornet, J. Aulin, W. H. Gerstacker, X. Dong, and B. Ai, "Terahertz communication for vehicular networks," *IEEE Trans. on Vehicular Technology*, vol. 66, no. 7, pp. 5617–5625, 2017.

[47] C. Chaccour, R. Amer, B. Zhou, and W. Saad, "On the reliability of wireless virtual reality at terahertz (THz) frequencies," in *2019 10th IFIP International Conference on New Technologies, Mobility and Security (NTMS)*, 2019, pp. 1–5.

[48] C. Chaccour, M. N. Soorki, W. Saad, M. Bennis, and P. Popovski, "Can terahertz provide high-rate reliable low latency communications for wireless VR?" *arXiv preprint arXiv:2005.00536*, 2020.

[49] V. Petrov, M. Komarov, D. Moltchanov, J. M. Jornet, and Y. Koucheryavy, "Interference and SINR in millimeter wave and terahertz communication systems with blocking and directional antennas," *IEEE Trans. on Wireless Commun.*, vol. 16, no. 3, pp. 1791–1808, 2017.

[50] M. Di Renzo, "Stochastic geometry modeling and analysis of multi-tier millimeter wave cellular networks," *IEEE Trans. on Wireless Commun.*, vol. 14, no. 9, pp. 5038–5057, 2015.

[51] I. S. Gradshteyn and I. M. Ryzhik, *Table of integrals, series, and products.* Academic press, 2014.

[52] H. Tabassum, E. Hossain, M. J. Hossain, and D. I. Kim, "On the spectral efficiency of multiuser scheduling in RF-powered uplink cellular networks," *IEEE Trans. on wireless Commun.*, vol. 14, no. 7, pp. 3586–3600, 2015.

[53] S. Zarandi, A. Khalili, M. Rasti, and H. Tabassum, "Multi-objective energy efficient resource allocation and user association for in-band full duplex small-cells," *IEEE Trans. on Green Commun. and Networking*, 2020.

[54] T. K. Thuc, E. Hossain, and H. Tabassum, "Downlink power control in two-tier cellular networks with energy-harvesting small cells as stochastic games," *IEEE Trans. on Commun.*, vol. 63, no. 12, pp. 5267–5282, 2015.

[55] A. Khalili, S. Akhlaghi, H. Tabassum, and D. W. K. Ng, "Joint user association and resource allocation in the uplink of heterogeneous networks," *IEEE Wireless Commun. Letters*, vol. 9, no. 6, pp. 804–808, 2020.

Appendix A

A.1 Proof of Lemma 1

Given the event when user is associated to TBS in the tier $k = T$, then the conditional PDF of the distance from the connected TBS can be obtained as follows:

$$f_{r_T}(r_T) = \frac{1}{A_T} \frac{d\mathbb{P}(d_0 > r_T, k = T)}{dd_0}. \tag{A.1}$$

Subsequently, the joint PDF in the numerator can be derived as follows:

$$\begin{aligned}
\mathbb{P}(d_0 > r_T, k = \mathrm{T}) &= \mathbb{P}(d_0 > r_T, P_T^{\mathrm{rx}} > P_R^{\mathrm{rx}}), \\
&= \int_{r_T}^{\infty} \mathbb{P}(P_T^{\mathrm{rx}} > P_R^{\mathrm{rx}}) f_{d_0}(d_0) dd_0, \\
&= \int_{r_T}^{\infty} \mathbb{P}\left(P_T \gamma_T \frac{\exp(-K_a d_0)}{d_0^2} > P_R \gamma_R r_0^{-\alpha} \right) f_{d_0}(d_0) dd_0, \\
&\overset{(a)}{=} \int_{r_T}^{\infty} 2\pi\lambda_T d_0 \, e^{\left(-\pi\lambda_T d_0^2 - \pi\lambda_R (d_0^2 Q)^{\frac{2}{\alpha}} \exp\left(\frac{2K_a d_0}{\alpha}\right)\right)} dd_0,
\end{aligned} \tag{A.2}$$

where (a) follows from substituting $\mathbb{P}(P_T^{\mathrm{rx}} > P_R^{\mathrm{rx}})$ in (3.14), and $f_{d_0}(d_0) = 2\pi\lambda_T d_0 e^{-\pi\lambda_T d_0^2}$. Now the final value of $f_{r_T}(r_T)$ is obtained by replacing (A.2) into (A.1).

A.2 Proof of Lemma 3

The event $k = R$ is defined as the event when user is associated to RBS, then the conditional PDF of the distance from the tagged RBS can be derived as follows:

$$f_{r_R}(r_R) = \frac{1}{A_R} \frac{d\mathbb{P}(r_0 > r_R, k = R)}{dr_R}. \tag{A.3}$$

Subsequently, the joint PDF in the numerator of (A.3) can be derived as follows:

$$\begin{aligned}
\mathbb{P}(r_0 > r_R, k = \mathrm{R}) &= \mathbb{P}(r_0 > r_R, P_R^{\mathrm{rx}} > P_T^{\mathrm{rx}}), \\
&= \int_{r_R}^{\infty} \mathbb{P}(P_R^{\mathrm{rx}} > P_T^{\mathrm{rx}}) f_{r_0}(r_0) dr_0, \\
&= \int_{r_R}^{\infty} \mathbb{P}\left(P_R \gamma_R r_0^{-\alpha} > P_T \gamma_T \frac{\exp(-K_a d_0)}{d_0^2} \right) f_{r_0}(r_0) dr_0, \\
&\overset{(a)}{\approx} \int_{r_R}^{\infty} \mathbb{P}\left(P_R \gamma_R r_0^{-\alpha} > P_T \gamma_T d_0^{-2-\mu} \right) f_{r_0}(r_0) dr_0, \\
&= \int_{r_R}^{\infty} 2\pi\lambda_R r_0 \exp\left(-\pi\lambda_R r_0^2 - \pi\lambda_T \left(\frac{r_0^{\alpha}}{Q} \right)^{\frac{2}{2+\mu}} \right) dr_0,
\end{aligned} \tag{A.4}$$

where the approximation $r_T^2 \exp(K_a r_T)$ with $r^{2+\mu}$ and the efficient choice of correcting factor μ (as discussed in Section III) help to derive the expression in step (a). Finally, substituting (A.4) in (A.1) yields $f_{r_T}(r_T)$ as given in **Lemma 1**. Here, $f_{r_0}(r_0) = 2\pi\lambda_R r_0 \exp(-\pi\lambda_R r_0^2)$ and $f_{d_0}(d_0) = 2\pi\lambda_R d_0 \exp(-\pi\lambda_R d_0^2)$.

Appendix B

B.1 Proof of Lemma 2

It can be observed from Fig. 2(a) that the vertical HO between RF and THz tiers does not occur if all BSs within these two tiers except tagged BS (i.e., TBS) are situated outside the area $|B' \setminus B' \cap A'|$. When the distance is r_T and the direction (or angle) of user movement is θ, there will be no HO from the serving TBS with probability as follows:

$$\begin{aligned}\mathbb{P}(\overline{H}_T|r_T,\theta) =& \mathbb{P}(N(|B' \setminus B' \cap A'|) = 0|T_T \neq T_R) \\ &+ \mathbb{P}(N(|B \setminus B \cap A|) = 0|T_T = T_R),\end{aligned} \tag{B.1}$$

where $\overline{H}_T$ is the complement of H_T and $N(\cdot)$ presents the number of BSs within a particular area. Here, T_T and T_R simplifies the THz and RF tier, respectively. After averaging over r_T and θ, the overall HOP, $\mathbb{P}(H_T)$. The first expression in Eq. (B.1) states the vertical HO and the second expression is the horizontal HO. Finally,

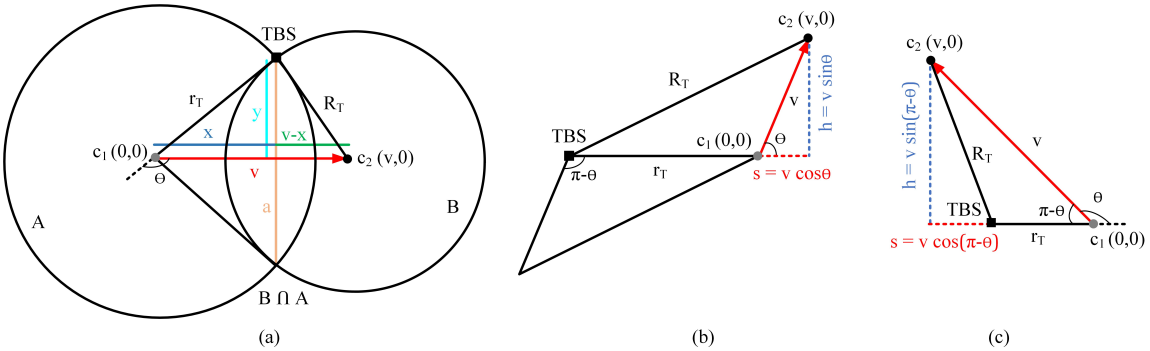

Figure B.1: (a) Geometrical illustration of r_T, R_T, v and θ, (b) $0 \leq \theta < \frac{\pi}{2}$, (c) $\frac{\pi}{2} \leq \theta \leq \pi$.

applying the null property of the PPP, I have,

$$\begin{aligned}\mathbb{P}(\overline{H}_T|r_T,\theta) &= \exp\left(\sum_{i\epsilon T,R} \lambda_i \cdot |B' \setminus B' \cap A'|\right), \\ &= \exp\left(\lambda_T \cdot |B \setminus B \cap A| + \lambda_R \cdot |B' \setminus B' \cap A'|\right). \end{aligned} \tag{B.2}$$

Here, $B = \pi R_T^2$, $B' = \pi R_R'^2$. Using the Pythagoras theorem from Fig. (B.1.a), following two equations can be generated:

$$y^2 = R_T^2 - x^2 \tag{B.3}$$

$$r_T^2 = (x - v)^2 + y^2 \tag{B.4}$$

Combining Eq. (B.3) and Eq. (B.4) as follows:

$$r_T^2 = (x - v)^2 + R_T^2 - x^2$$

$$\Rightarrow r_T^2 = x^2 - 2xv + v^2 + R_T^2 - x^2$$

$$\Rightarrow 2xv = R_T^2 + v^2 - r_T^2$$

$$\Rightarrow x = \frac{R_T^2 + v^2 - r_T^2}{2v} \tag{B.5}$$

Putting B.5 in B.3:

$$y^2 = R_T^2 - \frac{\left(R_T^2 + v^2 - r_T^2\right)^2}{4v^2}$$

Again from Fig. (B.1.a), the cord length is:

$$\begin{aligned} a &= 2y \\ &= \frac{1}{v}\sqrt{4R_T^2v^2 - (R_T^2 + v^2 - r_T^2)} \\ &= \frac{1}{v}\sqrt{(r_T + R_T - v)(r_T + R_T + v)(v + r_T - R_T)(v - r_T + R_T)} \end{aligned} \tag{B.6}$$

The area of the asymmetric lens in any circle can be derived using the formula for the circular segment of radius R_T, cord length a, and triangular height x with angle θ as follows:

$$\begin{aligned} A_{\text{asymmetric}-\text{lens}}(R_T, x) &= A_{\text{sector}} - A_{\text{iso}-\text{triangle}} \\ &= \left[\left(\frac{\beta}{2\pi}\right)\pi R_T^2\right] - \left[\frac{1}{2}ax\right] \\ &= R_T^2\left(\frac{\beta}{2}\right) - \frac{1}{2}ax \\ &= R_T^2\cos^{-1}\left(\frac{x}{R_T}\right) - \frac{1}{2}ax \end{aligned} \tag{B.7}$$

Therefore, adding two asymmetric lens from Fig. (B.1.a), will provide the area $|B \cap A|$ as follows:

$$\begin{aligned}
|B \cap A| &= A_{\text{asymmetric-lens}}(R_T, x) + A_{\text{asymmetric-lens}}(R_T, v-x) \\
&= \left[R_T^2 \cos^{-1}\left(\frac{x}{R_T}\right) - \frac{1}{2}ax\right] + \left[r_T^2 \cos^{-1}\left(\frac{v-x}{r_T}\right) - \frac{1}{2}a(v-x)\right] \\
&= R_T^{2\,-1}\left(\frac{x}{R_T}\right) + r_T^2 \cos^{-1}\left(\frac{v-x}{r_T}\right) - \frac{1}{2}av \\
&= R_T^2 \cos^{-1}\left(\frac{R_T^2 + v^2 - r_T^2}{2R_T v}\right) + r_T^2 \cos^{-1}\left(\frac{r_T^2 + v^2 - R_T^2}{2r_T v}\right) \\
&- \frac{1}{2}\sqrt{(r_T + R_T - v)(r_T + R_T + v)(v + r_T - R)(v - r_T + R_T)}
\end{aligned} \tag{B.8}$$

Here, $v - x = \frac{r_T^2 + v^2 - R_T^2}{2v}$. From Fig. (B.1.b),

$$\begin{aligned}
R_T^2 &= h^2 + (r_T + s)^2 \\
&= v^2 \sin^2\theta + r_T^2 + 2r_T v \cos\theta + v^2 cos^2\theta \\
&= v^2 + r_T^2 + 2r_T v \cos\theta
\end{aligned}$$

$$\Rightarrow -\cos\theta = \frac{r_T^2 + v^2 - R_T^2}{2r_T v} \tag{B.9}$$

Now, for both Fig. (B.1.a) and Fig. (B.1.b), the second term of the Eqn. (B.8) stated using cosign formula as follows:

$$\begin{aligned}
r_T^2 &= R_T^2 + v^2 - 2R_T v \cos(\theta - \varphi) \\
&= R_T^2 + v^2 + 2R_T v \cos(\pi - (\theta - \varphi)) \\
&= R_T^2 + v^2 + 2R_T v \cos\left(\pi - \theta + \sin^{-1}\left(\frac{v\sin\theta}{R_T}\right)\right)
\end{aligned} \tag{B.10}$$

Here, $\sin\varphi = \frac{v\sin\theta}{R}$

$$\begin{aligned}
&\frac{1}{2}\sqrt{(r_T + R_T - v)(r_T + R_T + v)(v + r_T - R_T)(v - r_T + R_T)} \\
&= \frac{1}{2}\sqrt{[(r_T + v)^2 - R_T^2][R_T^2 - (r_T - v)^2]} \qquad \text{(B.11)} \\
&= \frac{1}{2}\sqrt{2r_T v[1 - \cos\theta]2r_T v[1 + \cos\theta]} \\
&= r_T v\sin\theta \qquad \text{(B.12)}
\end{aligned}$$

Putting Eq.(B.9), and Eq.(B.11) in Eq.(B.8) with using the identity $\cos^{-1}(-\cos(\sigma)) = \pi - \sigma$, the part of expression in Eq. (B.2), $|B \cap A|$ can be easily determined as follows:

$$|B \cap A| = R_T^2\theta_1 + r_T^2(\pi - \theta) - r_T v\sin\theta \qquad \text{(B.13)}$$

Now, generally

$$\begin{aligned}
|B \backslash B \cap A| &= |B| - |B \cap A| \\
&= \pi R_T^2 - \left(R_T^2\theta_1 + r_T^2(\pi - \theta) - r_T v\sin\theta\right) \\
&= R_T^2(\pi - \theta_1) + r_T v\sin\theta - r_T^2(\pi - \theta) \qquad \text{(B.14)}
\end{aligned}$$

According to the Fig. (3.2.a), the common area between two intersecting circles of radii r_T and R_T is S_T. For horizontal no HO in TBS, Eq.(B.14) can be re-write as:

$$\begin{aligned}
\mathbb{P}(\overline{H}_{T,T}|r_T, \theta) &= \exp\left(-\lambda_T(R_T^2(\pi - \theta_1^T) + r_T\, v\, \sin\theta - r_T^2(\pi - \theta))\right) \\
&= \exp(-\lambda_T S_T)
\end{aligned}$$

Here, the value of $\theta_1^T = \theta - \sin^{-1}\left(\frac{v\sin\theta}{R_T}\right)$, which is true when the value of θ lies between 0 and $\frac{\pi}{2}$. According to Fig. (B.1.c), when the value of θ is in between $\frac{\pi}{2}$ and π then r is no longer greater than $\{v\cos(\pi-\theta)\}$ or in other words, $v\cos(\pi-\theta) > r$. For $\frac{\pi}{2} \leq \theta \leq \pi$ from [26], $\left\{\sin^{-1}\left(\frac{v\sin\theta}{R_T}\right)\right\}$ in θ_1^T will be replaced by $\left\{\pi - \sin^{-1}\left(\frac{v\sin\theta}{R_T}\right)\right\}$. Therefore, I define a new term C_T with modified θ_1^T to substitute the term S_T as follows:

$$\begin{aligned}\mathbb{P}(\overline{H}_{T,T}|r_T,\theta) &= \exp\left(-\lambda_T(R_T^2(\pi-\theta_1^{'T}) + r_T\, v\sin\theta - r_T^2(\pi-\theta))\right)\\ &= \exp(-\lambda_T C_T)\end{aligned}$$

According to definition, vertical-HO made between two BSs in two different tiers. Here, RBS is directly responsible to cause vertical-HO in TBS. For vertical no HO in TBS with the intensity of RBSs (i.e., λ_R), the common area between two intersecting circles from radii r'_R and R'_R is S'_T, Eq.(B.14) can be re-write as:

$$\begin{aligned}\mathbb{P}(\overline{H}_{T,R}|r_T,\theta) &= \exp\left(-\lambda_R(R_T^{'2}(\pi-\theta_3^T) + r_T^{'}\, v\sin\theta_2^T - r_T^{'2}(\pi-\theta_2^T))\right)\\ &= \exp(-\lambda_R S_T^{'})\end{aligned}$$

For $\frac{\pi}{2} \leq \theta_2^T \leq \pi$ from [26], $\left\{\sin^{-1}\left(\frac{v\sin\theta_2^T}{R'_R}\right)\right\}$ in θ_3^T will be replaced by $\left\{\pi - \sin^{-1}\left(\frac{v\sin\theta_2^T}{R'_R}\right)\right\}$. Therefore, I define a new term C'_T with modified θ_3^T to substitute the term S'_T as:

$$\begin{aligned}\mathbb{P}(\overline{H}_{T,R}|r_T,\theta) &= \exp\left(-\lambda_R(R_T^{'2}(\pi-\theta_3^{'T}) + r_T^{'}\, v\sin\theta_2^T - r_T^{'2}(\pi-\theta_2^T))\right)\\ &= \exp(-\lambda_R C_T^{'})\end{aligned}$$

where $R_T^2 = r_T^2 + v^2 - 2r_T v\cos(\pi-\theta)$, $R'_R = (R_T)^{\frac{2}{\alpha}}\, e^{\frac{K_a\, R_T}{\alpha}} \left(\frac{P_R^{tx} Q}{P_T^{tx}}\right)^{\frac{1}{\alpha}}$, $r'_R = (r_T)^{\frac{2}{\alpha}}\, e^{\frac{K_a\, R_T}{\alpha}} \left(\frac{P_R^{tx} Q}{P_T^{tx}}\right)^{\frac{1}{\alpha}}$, $\theta_1^T = \theta - \sin^{-1}\left(\frac{v\sin\theta}{R_T}\right)$, $\theta_2^T = \cos^{-1}\left(\frac{r_R'^2 + v^2 - R_R'^2}{2r'_R v}\right)$, $\theta_3^T = \theta - \sin^{-1}\left(\frac{v\sin\theta}{R'_R}\right)$. The no HOP between TBS and RBS will be determined by taking the average over r_T and θ as follows:

$$\begin{aligned}\mathbb{P}(\overline{H}_T) &= \mathbb{E}_\theta\left[\mathbb{E}_{r_T}\left[\mathbb{P}(\overline{H}_T|r_T,\theta)\right]\right] \\ &= \frac{1}{\pi}\int_0^\pi \int_0^\infty \mathbb{P}(\overline{H}_T|r_T,\theta)\, f_{r_T}(r_T) dr_T d\theta \end{aligned} \tag{B.15}$$

Therefore, in TBS, the overall HOP $\mathbb{P}[\mathrm{H_T}]$ with applying correction [26] as follows:

$$\begin{aligned}\mathbb{P}(\overline{H}_T) =& \frac{1}{\pi}\left(\int_{\theta=0}^{\frac{\pi}{2}} \int_{r_T=0}^{\infty} f_{r_T}(r_T)\exp\left(-\lambda_T S_T - \lambda_R S'_T\right) dr_T d\theta \right. \\ &+ \int_{\theta=\frac{\pi}{2}}^{\pi} \int_{r_T=0}^{v\cos(\pi-\theta)} f_{r_T}(r_T)\exp\left(-\lambda_T C_T - \lambda_R C'_T\right) dr_T d\theta \\ &\left. + \int_{\theta=\frac{\pi}{2}}^{\pi} \int_{r_T=v\cos(\pi-\theta)}^{\infty} f_{r_T}(r_T)\exp\left(-\lambda_T S_T - \lambda_R S'_T\right) dr_T d\theta \right),\end{aligned}$$

Appendix C

C.1 Proof of Lemma 4

The vertical HO between THz and RF tiers does not occur if all the BSs of these two tiers except tagged RBSs are located outside the area $|A' \setminus A' \cap B'|$. When the distance is r_R and the direction (or angle) of the user movement is θ, there will be no HO from the serving RBS with probability as follows:

$$\begin{aligned}\mathbb{P}(\overline{H}_R|r_R,\theta) =& \mathbb{P}(N(|A' \setminus A' \cap B'|) = 0|T_R \neq T_T) \\ &+ \mathbb{P}(N(|A \setminus A \cap B|) = 0|T_R = T_T),\end{aligned} \tag{C.1}$$

where $\overline{H}_R$ is the complement of H_R and $N(\cdot)$ depicts the number of BSs within a particular area. The first expression in Eq. (C.1) states the vertical HO and the second expression determines the horizontal HO. Finally, applying the null property of the PPP, I have:

$$\begin{aligned}\mathbb{P}(\overline{H}_R|r_R,\theta) &= \exp\left(\sum_{j\epsilon R,T} \lambda_j \cdot |A' \setminus A' \cap B'|\right), \\ &= \exp\left(\lambda_R \cdot |A \setminus A \cap B| + \lambda_T \cdot |A' \setminus A' \cap B'|\right).\end{aligned} \tag{C.2}$$

Here, $A = \pi R_R^2$, $A' = \pi R_T'^2$. Likewise appendix B, it can be determined the two-parts of Eq. (C.2), i.e., $|A \cap B|$ and $|A' \cap B'|$ can be given as in the following:

$$\begin{aligned}|A \cap B| =& R_R^2 \cos^{-1}\left(\frac{R_R^2 + v^2 - r_R^2}{2R_R^2 v}\right) + r_R^2 \cos^{-1}\left(\frac{r_R^2 + v^2 - R_R^2}{2r_R^2 v}\right) \\ & - \frac{1}{2}\sqrt{(r_R + R_R - v)(r_R + R_R + v)(v + r_R - R_R)(v - r_R + R_R)}, \\ =& R_R^2\, \theta_1^R + r_R^2(\pi - \theta) - r_R\, v \sin\theta. \end{aligned} \tag{C.3}$$

$$\begin{aligned}|A' \cap B'| =& R_T'^2 \cos^{-1}\left(\frac{R_T'^2 + v^2 - r_T'^2}{2R_T'^2 v}\right) + r_T'^2 \theta_2^R \\ & - \frac{1}{2}\sqrt{(r_T' + R_T' - v)(r_T' + R_T' + v)(v + r_T' - R_T')(v - r_T' + R_T')}, \\ =& R_T'^2\, \theta_3^R + r_T'^2(\pi - \theta_2^R) - r_T'\, v \sin\theta_2^R. \end{aligned} \tag{C.4}$$

The common area between two intersecting tiers can be calculated from Eq. (C.3) and Eq. (C.4), where $R_R^2 = r_R^2 + v^2 - 2r_R\, v\cos(\pi - \theta)$, $R_T' = \left[(R_R)^\alpha \left(\frac{P_T^{tx}}{P_R^{tx} Q}\right)\right]^{\frac{1}{2+\mu}}$, $r_T' = \left[(r_R)^\alpha \left(\frac{P_T^{tx}}{P_R^{tx} Q}\right)\right]^{\frac{1}{2+\mu}}$, $\theta_1^R = \theta - \sin^{-1}\left(\frac{v\sin\theta}{R_R}\right)$, $\theta_2^R = \cos^{-1}\left(\frac{r_T'^2 + v^2 - R_T'^2}{2r_T' v}\right)$, $\theta_3^R = \theta - \sin^{-1}\left(\frac{v\sin\theta}{R_T'}\right)$. According to the Fig. (3.2.b), the common area between two intersecting circle with radii r_R and R_R is S_R. Here, the value of $\theta_1^R = \theta - \sin^{-1}\left(\frac{v\sin\theta}{R_R}\right)$, which is true when the value of θ lies between 0 and $\frac{\pi}{2}$. Similar way as Fig. (B.1.c), when $\frac{\pi}{2} \le \theta \le \pi$ then, $v\cos(\pi - \theta) > r$. For $\frac{\pi}{2} \le \theta \le \pi$ from [26], θ_1^R becomes $\left\{\theta - \pi + \sin^{-1}\left(\frac{v\sin\theta}{R_R}\right)\right\}$. Therefore, a new term C_R is defined by modifying θ_1^R to substitute the term S_R.

Likewise, the common area between two intersecting circles of radii r_T' and R_T' is S_R', and later term C_R' with modified θ_3^R to substitute the term S_R'.